UC-213

LBL-28164

Lawrence Berkeley Laboratory

UNIVERSITY OF CALIFORNIA

APPLIED SCIENCE DIVISION

Electrocatalysts for Oxygen Electrodes: Final Report

E. Yeager and S. Gupta

October 1989

For Reference

Not to be taken from this room

APPLIED SCIENCE DIVISION

LBL-28164
Copy 1
Bldg. 50 Library.

Prepared for the U.S. Department of Energy under Contract Number DE-AC03-76SF00098.

DISCLAIMER

This document was prepared as an account of work sponsored by the United States Government. While this document is believed to contain correct information, neither the United States Government nor any agency thereof, nor the Regents of the University of California, nor any of their employees, makes any warranty, express or implied, or assumes any legal responsibility for the accuracy, completeness, or usefulness of any information, apparatus, product, or process disclosed, or represents that its use would not infringe privately owned rights. Reference herein to any specific commercial product, process, or service by its trade name, trademark, manufacturer, or otherwise, does not necessarily constitute or imply its endorsement, recommendation, or favoring by the United States Government or any agency thereof, or the Regents of the University of California. The views and opinions of authors expressed herein do not necessarily state or reflect those of the United States Government or any agency thereof or the Regents of the University of California.

LBL-28164

ELECTROCATALYSTS FOR OXYGEN ELECTRODES

Final Report

October 1989

by

E. Yeager
S. Gupta

Case Center for Electrochemical Sciences
and the Department of Chemistry
Case Western Reserve University
Cleveland, Ohio 44106-2099

for

Technology Base Research Project
Applied Science Division
Lawrence Berkeley Laboratory
1 Cyclotron Road
Berkeley, California 94720

This work was supported by the Assistant Secretary for Conservation and Renewable Energy, Office of Energy Storage and Distribution, Energy Storage Division of the U.S. Department of Energy under Contract No. DE-AC03-76SF00098, Subcontract No. 4544410 with the Lawrence Berkeley Laboratory.

This report has been reproduced directly from the best available copy

PREFACE

This annual report is a comprehensive summary of the results. For details the reader is referred to the corresponding references. The following personnel have been involved in the research on a full or part time basis.

W. Aldred	Research Assistant
I. Bae	Graduate Student
R. Chen	Graduate Student
S. Gupta*	Senior Research Associate
J. Prakash	Graduate Student
B. Simic-Glavaski	Senior Research Associate
D. Tryk	Senior Research Associate
E. Yeager	Project Director

* Report prepared by S. Gupta

TABLE OF CONTENTS

PREFACE i

TABLE OF CONTENTS ii

I. SUMMARY 1

II. OBJECTIVES 7

III. INTRODUCTION 7

IV. ACCOMPLISHMENTS 8

A. Polymeric Sheet-Type Phthalocyanines 8

B. Spectroscopic Studies of Macrocycles 13

1. In-situ UV-visible Reflectance Spectroscopy of Adsorbed FeTsPc on Ag Electrode 13
2. Voltammetric and FTIR Spectroscopic Examination of CoTMPP Adsorbed on Smooth Surfaces 20
3. In-situ FTIRRAS Studies of FeTsPc on Ag and OPG Electrodes 29

C. Controlled Poisoning of Transition Metal Macrocycles 30

1. Fe- and Co-TsPc 32
2. Fe- and Co-TMPP 37

D. Pyrochlore Electrocatalysts 41

1. Synthesis 41
2. X-ray Diffraction and XPS Studies 41
3. TGA Studies 42
4. Peroxide Decomposition 43

E. Heat-treated Polymeric Phthalocyanine and Pyrochlore Catalysts 47

1. Heat-treated Polymeric Phthalocyanine Catalysts 47
2. Heat-treated Pyrochlore Catalyst 49

F. Bifunctional Oxygen Electrodes and Improved Catalyst Supports 49

1. Bifunctional Electrodes 49
2. Improved Catalyst Supports 55

V FUTURE WORK 58

VI REFERENCES 59

I. SUMMARY

The overall objective of this research was an in-depth understanding of the factors controlling O_2 reduction and generation on various electrocatalysts and the use of this understanding to identify much higher activity, stable catalysts. The specific aspect of catalyst systems investigated under the LBL project include:

1. Polymeric sheet-type phthalocyanines
2. Spectroscopic studies of macrocycles
3. Controlled poisoning of transition-metal macrocycles
4. Pyrochlore electrocatalysts
5. Heat-treated polymeric phthalocyanines and pyrochlore catalysts
6. Bifunctional O_2 electrodes and improved catalyst supports

New features of the work during the past year included:

- controlled poisoning of macrocycles by CN^-
- in-situ and ex-situ FTIR studies of macrocycles adsorbed at monolayer levels on smooth substrates
- comparison of sheet-type polymeric and monomeric phthalocyanines in solution and adsorbed layers
- self-supported pyrochlore catalysts both for O_2 reduction and generation
- use of polymer coatings to stabilize catalysts such as pyrochlores for O_2 reduction and generation

1. Polymeric Sheet-Type Phthalocyanines

The research has continued on Fe- and Co- phthalocyanine (Pc) sheet polymers that have peripheral acid groups. Polymeric FePc adsorbed at monolayer level on OPG was found to support the 4-e^- reduction of O_2 to OH^- similar to the monomeric FePc's but is expected to be more stable. The voltammetric and O_2 reduction electrocatalytic studies on polymeric Pc's have also been extended to the high area forms using the thin porous coating (TPC) electrode technique.

These studies were undertaken with a view to checking our models for the interaction of O_2 with the transition metal in the macrocycle and the structural factors which may play a rôle in the catalytic activity for O_2 reduction.

UV-visible absorption spectroscopic studies for monomeric and polymeric iron phthalocyanines were carried out in DMF, DMA and DMSO solutions. The effect of the peripheral substituents in the phthalocyanine ring as well as environmental conditions, such as solvent, air and light, on the spectral properties were investigated. This provides essential information on the electronic properties of iron complexes in the solution phase.

Efforts continue to image directly phthalocyanines including polymeric phthalocyanines adsorbed on HOPG in monolayer coverages using scanning tunelling microscopy (STM) (Nanoscope II at B. P. America). Transmission electron microscopy (TEM) studies are being carried out using a JEOL 4000 having a resolution of ~1.35 A in our Materials Science and Engineering Department.

2. Spectroscopic Studies on Macrocycles

In-situ UV-visible spectroscopic studies for monolayer-adsorbed FeTsPc on Ag were made to obtain further insight into the molecular orientation of the adsorbed macrocycles on metal surfaces and to have more understanding about the corresponding electrochemical behavior.

The normalized reflectance spectra of FeTsPc adsorbed at a monolayer level on Ag surface exhibited features at 636 and 677 nm which compared very favorably with the solution-phase transmission spectrum for FeTsPc in the same electrolyte. The spectral features are very similar to those reported earlier by CWRU for FeTsPc and CoTsPc on a Pt surface and the basal plane of HOPG. This study supports the perpendicular-ligand surface orientation proposed by the CWRU group.

FTIRRAS spectra of CoTMPP (1.5×10^{-10} moles/cm^2, or ~10 monolayers) on Ag, Ni and HOPG were obtained ex-situ. These samples were prepared by evaporation of solvent after applying CoTMPP dissolved in acetone. The spectra for CoTMPP on Ag, Ni and HOPG were similar to each other and not much different from that of the bulk material. When CoTMPP (dissolved in acetone) was injected into the electrochemical cell containing HOPG, a strong interaction with HOPG surface under potential control was obtained. The adsorption isotherm of CoTMPP in acetone was obtained on HOPG. The voltammograms obtained with acetone solution, injected into N_2-purged H_2SO_4 solution (~1×10^{-6} M CoTMPP in 0.05 M H_2SO_4, 1:100 acetone-water) reached a steady state in a half-hour to give very similar features to those of CoTsPc adsorbed on HOPG. The adsorption showed Langmuirian behavior.

Three adsorbed samples prepared by different methods were examined with FTIRRAS to obtain insight into the orientation of CoTMPP on the basal plane of HOPG. The samples were thoroughly washed with pure water prior to the spectroscopic measurements. The samples prepared by evaporation of the solvent after applying CoTMPP dissolved in acetone on the surface showed a irreversible Co(II)/Co(III) peak which is probably due to the aggregation of CoTMPP which formed during evaporation. The potential difference of the reversible Co(II)/Co(III) couple from samples prepared by injecting CoTMPP dissolved in acetone into the electrochemical cell may be due to the effects of anions or pH. The aggregation of CoTMPP from evaporated samples is also evident in the corresponding FTIRRAS spectrum since all the vibrational peaks for the bulk sample are different from the spectra for the injected sample. Two common peaks were observed at 806 and 667 cm^{-1} in the three spectra which correspond to C-H stretch and ring vibration of either benzene and pyrrole, respectively. The reason for the differences in the spectral features of the three adsorbed

samples are discussed in terms of the orientation of CoTMPP on the surface.

The adsorption of CoTMPP on Pt under aerobic and nonaerobic conditions was studied by injecting a specified amount of CoTMPP (~1 x 10^{-5} M) in 0.05 M H_2SO_4. The mechanism of O_2 penetration through the hydrophobic CoTMPP matrix and its reduction are discussed.

In-situ FTIRRAS spectra were also obtained for FeTsPc adsorbed at monolayer coverages on Ag and OPG electrodes in 0.1 M $HClO_4$ solution by using CWRU-built reflection-absorption optics with p-polarization at 70° incident angle and IBM-98 FTIR spectrometer. Preliminary results of the adsorbed FeTsPc on Ag indicate only the vibrational modes of the sulfonic acid groups and not the remainder of the macrocyclic ligand. One explanation is that the macrocycle may be oriented edge-on and only the sulfonic acid groups undergo significant vibrational change with the electric field in the interface. Consequently the other vibrational modes of the ligand are unchanged in the adsorbed state.

3. Controlled Poisoning of Transition-Metal Macrocycles

The effect of CN^-, capable of coordinating with the transition metal in the axial position, were examined to obtain further insight into the redox properties of the Fe and CoTsPc and TMPP as well as O_2 reduction electrocatalysis on these macrocycles. The major focus has been on the competitive interaction of CN^- and O_2 with the transition metal in the axial position. The results confirm that a strong axial interaction of O_2 with the transition metal is an important factor in O_2 electrocatalysis. This study has also helped in confirming the redox processes associated with the voltammetric peaks obtained with the transition-metal macrocycles.

4. Pyrochlore Electrocatalysts

Metallic oxides with the pyrochlore structure have attracted attention in recent years for their high catalytic activity for both O_2 reduction and gene-

ration. A series of pyrochlores with the general formula $Pb_2[Ru_{2-x}\ Pb_x]O_{6.5}$ [x = 0, 0.2, 0.3, 0.4, 0.6, 0.8 and 1.0] was synthesized at CWRU and characterized by x-ray diffraction and XPS.

The pyrochlore $Pb_2Ru_2O_{6.5}$, prepared by the alkaline solution method at ~80°C, was further heat-treated between 300°C to 500°C in flowing air and characterized by x-ray diffraction and XPS. The material is converted from a rather amorphous to a crystalline form. The TGA for $Pb_2Ru_2O_{6.5}$ showed a weight loss of 3 to 3.5% over the range 100 to 900°C due to the loss of chemically bound water.

Rate constants for peroxide decomposition were obtained by monitoring its concentration change using a rotating Au disk electrode. This was achieved by measuring the diffusion limiting current for peroxide oxidation ($HO_2^- + HO^- \longrightarrow O_2 + H_2O + 2\,\bar{e}$) on a Au disk. It was found that the apparent rate constant k' is directly proportional to the weight of the dispersed catalyst and follows the equation $d[H_2O_2]/dt = k_w(w/v)[H_2O_2]$ where k_w (ml $g^{-1}s^{-1}$) is the rate constant per gram of the catalyst in one ml of the solution. The values of k_w and the heterogeneous rate constant k_s per m^2 of the catalyst surface area (from BET measurements) were calculated. The effect of $[OH^-]$ concentration on H_2O_2 decomposition by the pyrochlore was also studied.

5. **Heat-Treated Polymeric Phthalocyanines and Pyrochlore**

Heat-treated (~800°C) polymeric Fe- and Co- phthalocyanines showed reduced activity for O_2 reduction as compared to the non-heat-treated or 400 °C heat-treated samples loaded on Vulcan XC-72 carbon. This is in contrast to the effect on heat-treated Fe- and Co-porphyrins and tetraazaannulenes. The reduced activity of the polymeric Pc's, heat-treated at ~800 °C, may be due to the decomposition of the polymer and loss of nitrogen which is an essential component along with the transition metal for catalytic activity.

The catalytic activity for O_2 reduction and generation on the pyrochlore $Pb_2Ru_2O_{6.5}$ is found to decrease with an increase in heat-treatment temperature of the catalyst. This may be as a result of the decrease in the surface area of the catalyst, which is heat-treated at higher temperatures. The stability of the heat-treated pyrochlore in concentrated alkaline solutions under anodic polarization, however, is expected to increase.

6. Bifunctional O_2 Electrodes and Improved Catalyst Supports

The pyrochlore structure was found to have high catalytic activity for both O_2 reduction and generation. The catalysts which were examined during the past year in the bifunctional mode have involved pyrochlores given in Table IV and also in combination with heat-treated macrocycles. Some of the pyrochlores were also used in a self-supporting mode without carbon. The carbon is generally considered to be unstable, particularly in O_2 generation.

A fluorinated anion exchange membrane (RAI 4035) which was pressed onto the electrolyte side of an electrode made from $Pb_2[Ru_{1.67}Pb_{0.33}]O_{6.5}$ and Shawinigan black (SB) carbon gave O_2 reduction behavior similar to that obtained without the membrane, but generation was considerably improved. A similar but smaller effect was observed for an electrode painted with a hydrogel suspension. This electrode performed very well at high cathodic current densities, giving the lowest polarization yet seen for a metal oxide catalyst at -800 mA/cm^2. The polymer layers help to retain the solution-phase component of the pyrochlore in the cathode structure and thus minimize surface chemical changes.

Efforts were made to find improved carbon supports. Preliminary experiments were also conducted with mildly fluorinated SB carbon obtained from Electrosynthesis Company, Inc., NY, as the support material. No improvements in O_2 reduction were observed with the mildly fluorinated SB carbon alone or

the CoTMPP-catalyzed mildly fluorinated SB carbon, as compared to the oxidized SB carbon alone or the CoTMPP-catalyzed SB carbon respectively. However, work is in progress to ascertain the effect of mild fluorination of high area carbons on the activity and stability of such carbons for O_2 reduction and generation, with and without catalysts present on such supports.

II. OBJECTIVES

The overall objectives of this research are

1. to develop an in-depth understanding of the factors controlling O_2 reduction and generation on various electrocatalysts, including transition-metal macrocycles and oxides;
2. to identify and develop much higher activity catalysts, both mono-functional and bifunctional;
3. to establish how the catalytic activity of an O_2 electrocatalyst depends on catalyst-support interactions and to identify stable catalyst supports for bifunctional O_2 electrodes.

III. INTRODUCTION

Over the past two decades a large research effort has been carried out on a wide range of catalysts for O_2 reduction in alkaline and acid electrolytes and to a lesser extent on O_2 generation, principally in alkaline electrolytes. Much of this research has been semi-Edisonian, guided by scientific hunches rather than an adequate understanding of the reactions of the electrocatalytic activity to the electronic and steric properties of the catalysts. Consequently, the emphasis on O_2 elelctrocatalytic research at CWRU is on achieving a new level of understanding for both O_2 reduction and generation in relation to the basic properties of the catalyst-electrolyte interface.

Research during the past year at CWRU involved work principally on the

following aspects:

A. Polymeric sheet-type phthalocyanines

B. Spectroscopic studies of macrocycles

C. Controlled poisoning of transition-metal macrocycles

D. Pyrochlore electrocatalysts

E. Heat-treated polymeric phthalocyanine and pyrochlore catalysts

F. Bifunctional oxygen electrodes and improved catalyst supports for both fuel cells and metal-air batteries.

IV. ACCOMPLISHMENTS

A. Polymeric Sheet-Type Phthalocyanines

The research has involved iron and cobalt phthalocyanine (Pc) sheet polymers that have peripheral acid groups. These studies were undertaken to examine further our models for the interaction of O_2 with the transition metal in the macrocycles and the structural factors which may play a role in O_2 electrocatalysis. Sheet-type polymeric FePc, preadsorbed on graphite disk in monolayer coverages, was found to support the 4-electron reduction of O_2 to OH^- in alkaline electrolyte similar to the monomeric FePc, iron tetrasulfonated phthalocyanine (FeTsPc) and iron tetrapyridinoporphyrazine (FeTPyPz) but is expected to be more stable than the monomeric phthalocyanines.

The voltammetric and O_2 reduction electrocatalytic studies on polymeric sheet-type phthalocyanines in the high area form were studied and compared with the corresponding high area forms of the monomeric phthalocyanines under similar conditions. These studies have been carried out with Fe- and Co-polymeric phthalocyanines on Vulcan XC-72 carbon in the form of a thin porous coating (TPC) on an ordinary pyrolytic graphite (OPG) rotating disk with Teflon as the binder in 0.1 M NaOH. These studies are of fundamental importance and provide information on the adsorption and orientation of polymer molecules on the substrate.

Voltammetric curves for the high-area monomeric and polymeric FePc on Vulcan C-72 carbon, adsorbed from DMF solution, were obtained. These studies indicate that the redox properties of the adsorbed polymeric phthalocyanines are similar to those of the corresponding monomers under similar conditions. However, there are some differences in the peak potentials, and the heights of the voltammetric peaks for the polymers are much lower than those of the corresponding monomers. These differences are probably due to the nature of the adsorption and orientation on the substrate (1). Evidence for such has been obtained by surface-enhanced Raman scattering (SERS) using a smooth polycrystalline Ag and a monolayer of the adsorbed polymeric phthalocyanine (2). The voltammetric results of the high-area form of the phthalocyanines are similar to the corresponding monolayer-adsorbed phthalocyanines on OPG.

Figure 1 shows the catalytic activity for O_2 reduction on polymeric cobalt and iron phthalocyanines in the high-area form in alkaline electrolyte. Although an exact analytical treatment of the kinetics from the current-potential curves obtained by the TPC technique is not yet available, this technique is quite useful in determining the catalytic activity for the high-area materials. Polymeric FePc is more active than polymeric CoPc for O_2 reduction and has almost the same activity as the monomeric form, particularly in the kinetic current region, and it may be more stable than the monomer.

Using a Perkin Elmer Lamda Array 3840 Spectrometer, a systematic study of the UV-visible absorption spectra were obtained for the monomeric iron phthalocyanines (Pc, TsPc and TPyPz) and polymeric FePc in DMF, DMA and DMSO solutions. The effect of the peripheral substituents in the phthalocyanine ring, as well as the environmental conditions (such as solvent, air and light), on the spectral properties were investigated. This provides essential information on the electronic properties of the iron complexes in the solution phase.

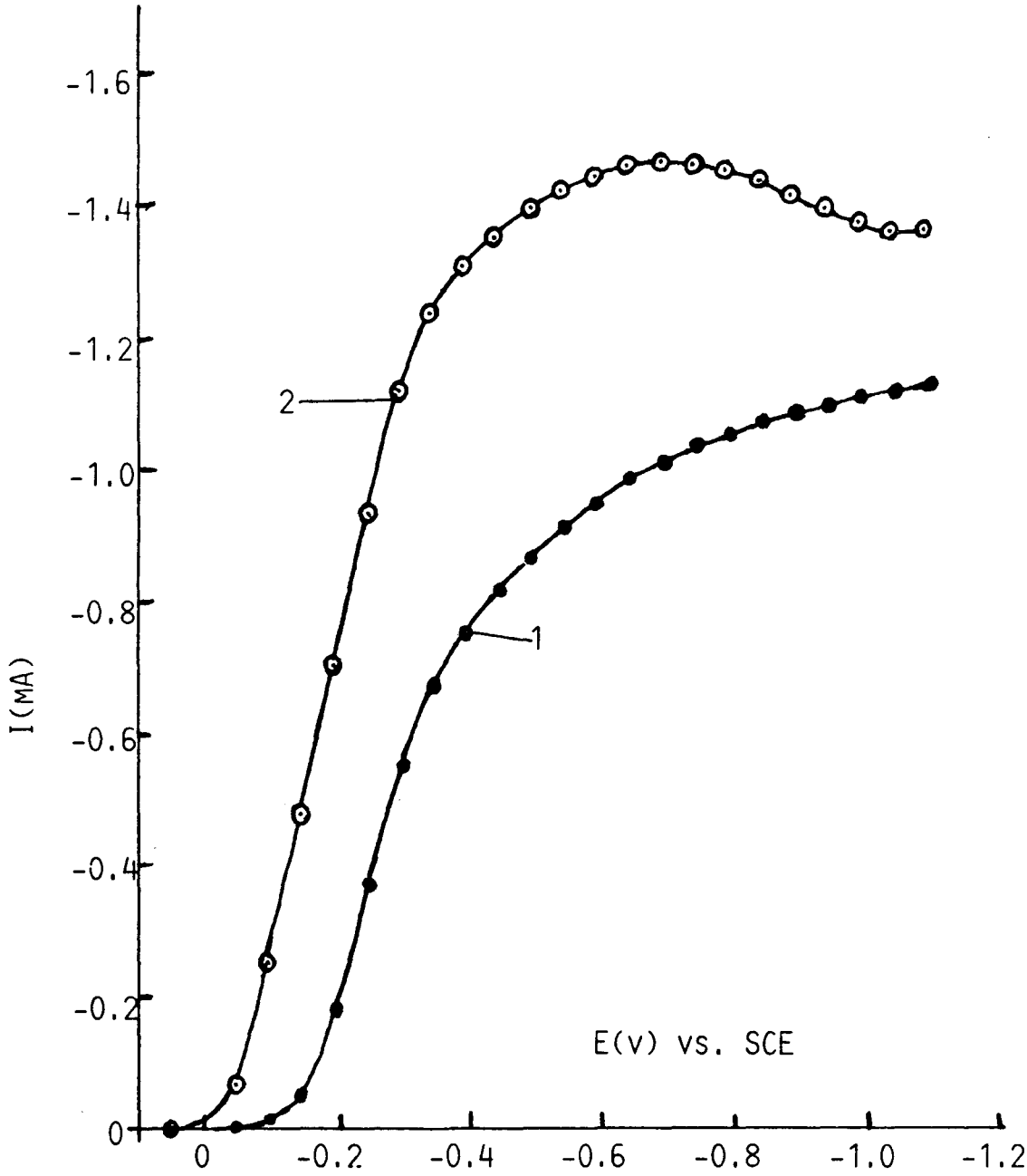

Fig. 1. Disk currents for O_2 reduction (1 atm) on a thin porous coating (TPC) electrode containing 5% polymeric phthalocyanines adsorbed on XC-72 carbon from DMF solution in 0.1 M NaOH. Electrode area, geometrical = 0.2 cm^2, 2500 rpm, room temperature, Teflon - 10%.

1 - Polymeric CoPc/XC-72
2 - Polymeric FePc/XC-72

The peripheral substituents cause the visible absorption spectra to red-shift (~10 nm) for FeTsPc relative to FePc (see Table I) under the comparable conditions. This is probably due to the increasing electron withdrawing capability of the sulfonic acid groups. For polymeric FePc a relatively large red-shift (~20 nm vs. M-FePc) is observed (see Table I). The visible and Soret bands are also broadened. Further work is in progress to explain these changes.

The absorption maxima shift to higher energies in the order: DMA ~DMF < DMSO. The monomeric iron complexes in DMF solution have an absorption band at 430-450 nm (Table I), which may be due to the strong coordinating ability of DMF with the monomer. However, the polymeric FePc does not show this band, probably because of the steric effect of the polymer (Table I).

When monomeric FePc solutions are exposed to air and light, the intensity of the absorption bands decreases and the absorption maxima shift slightly to higher energies. In contrast the polymeric complex is quite stable, and particularly in DMSO solution the absorption spectrum does not change even after one month. The reason for the change in intensity of the absorption bands and the slight shift in the absorption maxima for the monomeric FePc solutions under exposure to air and light with time is under investigation.

Recently Lippel et al. (3) used STM to image monomeric copper phthalocyanine molecules on a Cu(100) surface in an ultra high vacuum chamber at room temperature with monolayer coverage. The monolayer adsorbed phthalocyanines including the sheet-type polymeric phthalocyanines on highly ordered pyrolytic graphite (HOPG) were used *ex-situ* (in air) to study the structure of polymeric copper phthalocyanine by STM [Nanoscope II at B. P. America]. A crystalline structure was observed for polymeric Cu-phthalocyanine adsorbed on HOPG in multilayer coverage. Efforts continue to image directly phthalocyanines adsorbed on HOPG in monolayer coverage using STM. TEM studies of phthalocya-

TABLE I

Table: UV - Visible Spectra for Macrocycles in Organic Solvents

Sample	Solvent	Cell (cm)	Peak I	II	III	IV	V	VI	VII
FeTsPc	DMA	1.0	-	720 w	672 1.00	642 sh	608 sh	-	-
	DMF	1.0	-	-	667 1.00	642 sh	606 0.41	432 w	337 w
	DMSO	0.1	-	-	661 1.00	-	597 sh	-	336 1.02
FeTPyPz	DMA	1.0	-	-	657 0.37	642 1.00	583 0.33	451 0.36	345 0.70
	DMF	1.0	-	-	-	639 1.00	585 0.34	451 0.40	357 0.78
	DMSO	1.0	-	-	-	637 1.00	583 w	453 w	345 0.97
M-FePc	DMA	1.0	888 0.27	757 0.31	664 1.0	636 w	603 0.4	430 w	-
	DMF	1.0	822 0.13	-	660 1.00	635 w	600 0.31	430 0.28	-
	DMSO	1.0	-	-	654 1.00	-	594 sh	-	324 0.95
P-FePc	DMA	1.0	889 0.31	-	687 1.00	-	619 w	-	359 w
	DMF	1.0	891 0.41	-	685 1.00	-	623 w	-	357 w
	DMSO	1.0	-	-	673 1.00	-	608 w	-	351 1.12

Note: w = weak peaks sh = shoulder peaks

nines are being undertaken using a JEOL 4000 having a resolution of ~1.35 A in the Materials Science and Engineering Department. Polymeric sheet-type copper phthalocyanine was prepared and purified following the method of Achar et al. (4) and characterized using UV-visible spectroscopy and cyclic voltammetry.

B. Spectroscopic Studies of Macrocycles

1. In-Situ UV-Visible Absorption Spectroscopy of Adsorbed FeTsPc on Ag Electrode

To obtain further insight into the molecular orientation of adsorbed macrocycles on metal surfaces and gain a better understanding about the corresponding electrochemical behavior, an *in-situ* UV-visible spectroscopic set-up was implemented with the Cary-2300 (Varian) spectrometer. A spectro-electrochemical cell was designed (Fig. 2) and mounted in a reflection-absorption accessory (Harrick) in the spectrometer.

Figure 3 shows the UV-visible reflection-absorption spectrum of Ag in 0.05 M H_2SO_4 under open-circuit conditions, normalized by the absorption spectrum of the same sulfuric acid solution obtained in transmission mode. The absorption peak at 312 nm corresponds to the bulk plasmon absorption of silver and therefore its position is not altered by the applied potential. This is clearly seen in Fig. 4B (an expanded form of Fig. 4A) in which the normalized reflectivity curves obtained at different potentials cross at the position of the peak maximum. In contrast, the peak at 367 nm exhibits a strong potential dependence, especially at the most positive potentials examined (see Fig. 4). This is probably due to a shift in the absorption energy of surface plasmons, an effect that is more pronounced for rough surfaces [5] in electrolytes containing ions that can be specifically adsorbed on the electrode surface as is the case of sulfate and/or bisulfate [6, 7]. The jumps at 340 nm are artifacts as a result of the discontinuity in detection energy caused by the grating

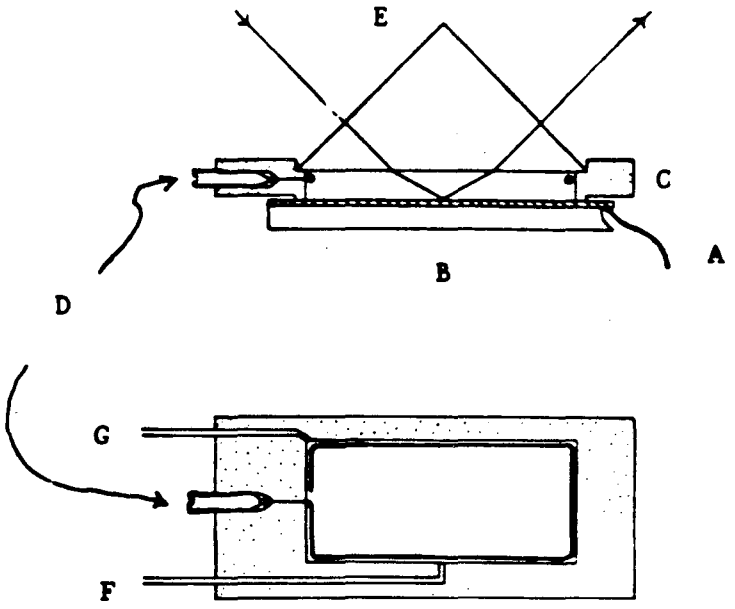

Fig. 2. *In situ* UV-Vis cell; A: Ag working electrode (2.6 cm^2), B: plastic back, C: Teflon body(0.35 cm electrolyte thickness), D: counter electrode and lead, E: quartz prism(45° isosceles), F: Teflon luggin capillary, G: Teflon solution outlet.

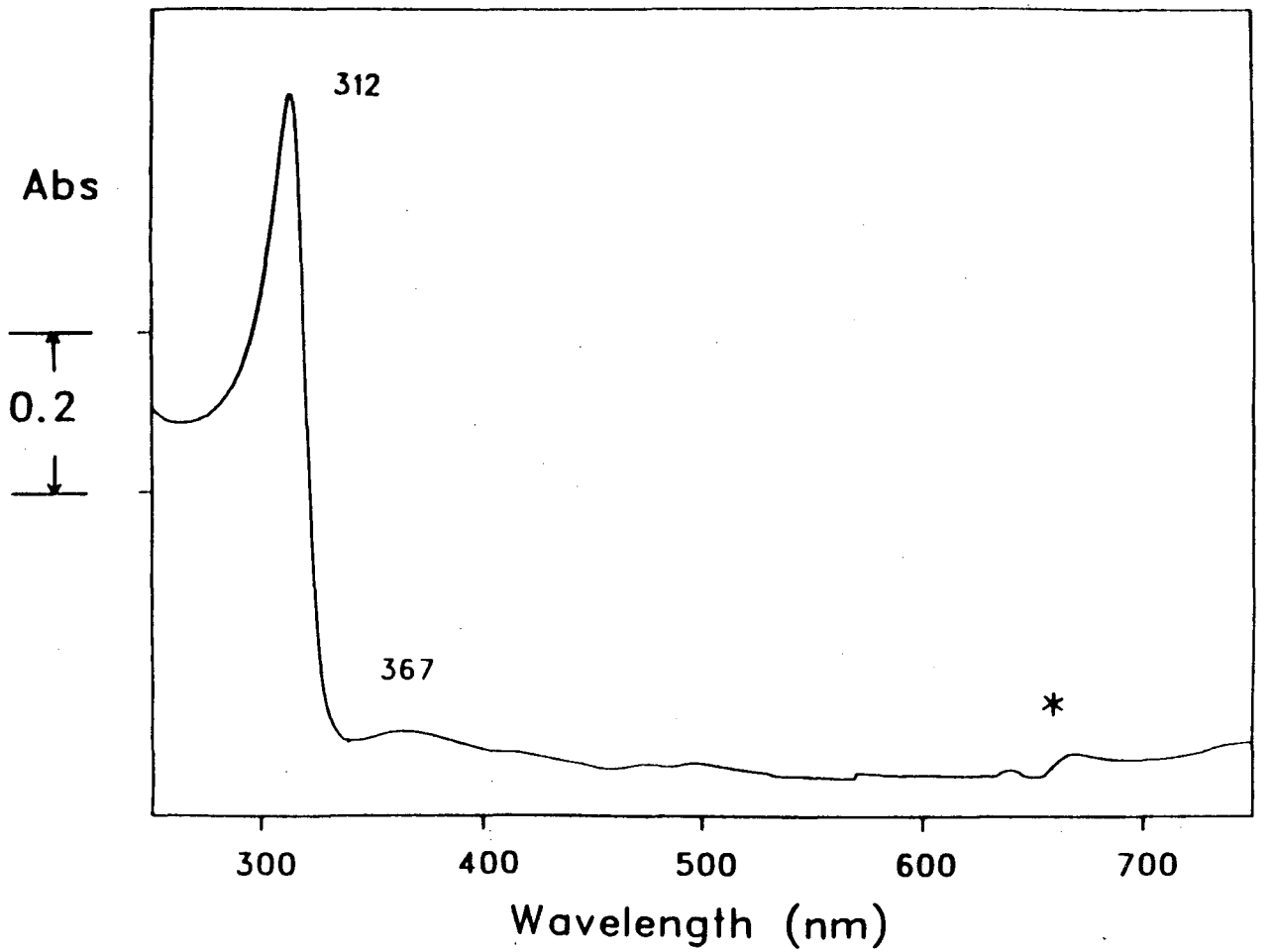

Fig. 3. UV-Vis reflectance spectrum of Ag in 0.05 M H_2SO_4 under open circuit conditions; normalized by the spectrum for the same sulfuric acid solution.
* Wood's anomaly

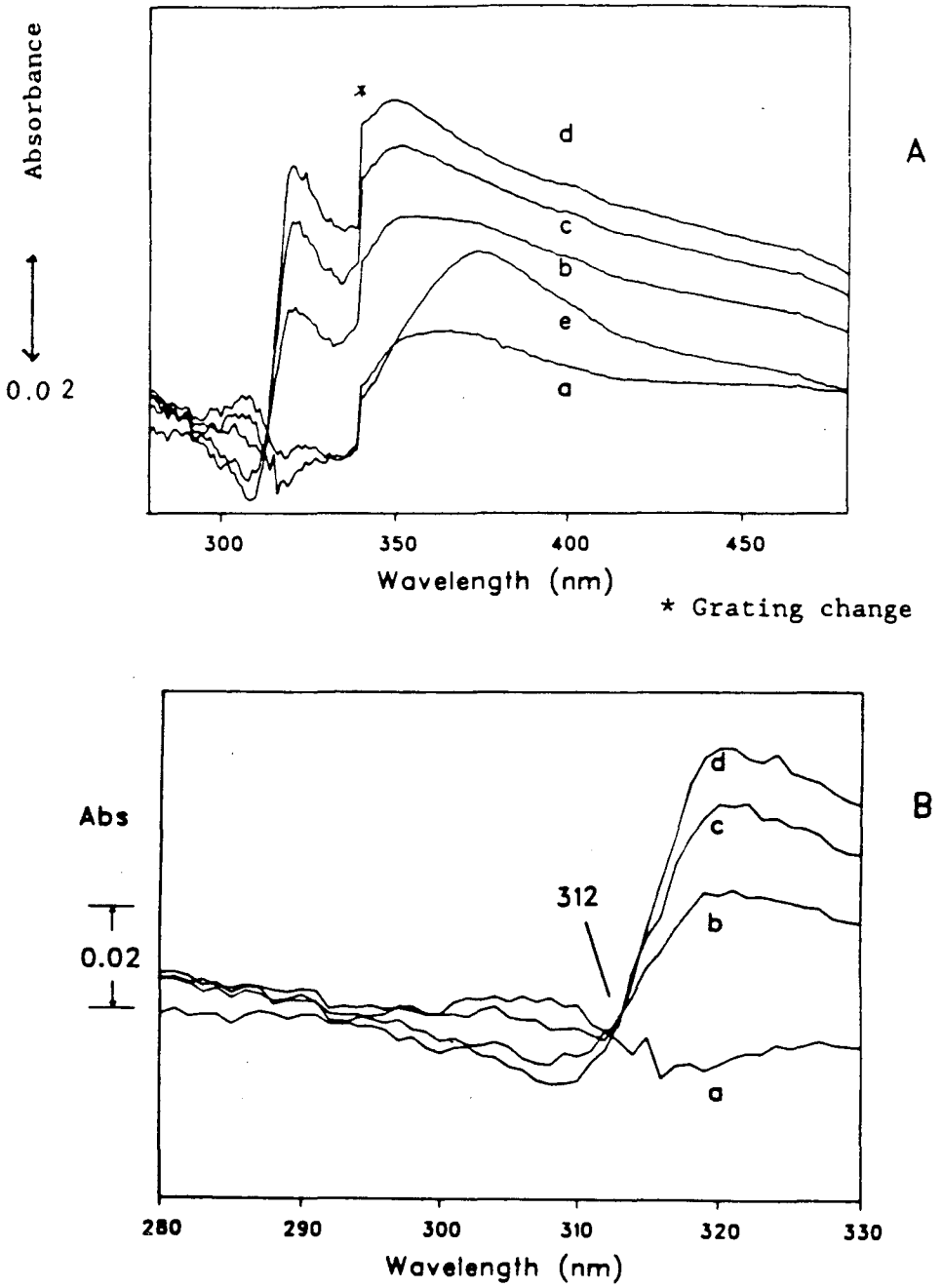

Fig. 4. *In situ* UV-Vis spectra of bare Ag in 0.05 M H_2SO_4 in the plasmon absorption region; nomalized by that at the open circuit potential;
A: a,0.0; b,-0.2; c,-0.3; d,-0.4; e,+0.15 V vs. SCE;
B: expanded scale, e:spectrum is omitted for clarity.

change in the spectrophotometer. It may be noted that the peaks observed around 650 nm are the result of the Wood' anomaly (ghosts) associated with the Cary 2300 instrument. The normalized reflectivity curves obtained at different potentials were stored in the computer and used later to normalize the spectra obtained for FeTsPc.

After collecting all the optical data for the bare Ag electrode, a 10^{-4} M FeTsPc solution was introduced into the cell. The cyclic voltammograms in 0.05 M H_2SO_4 obtained in the spectroelectrochemical cell before and after addition are shown as the dotted and the dashed curves in Fig. 5, respectively. After several potential sweeps the solution was replaced by the pure electrolyte solution, this voltammogram is shown as the solid curve. The voltammetry peaks at -0.1 and -0.35 V may be attributed to the redox couples involving molecular orbitals of the iron and the macrocycle ligand, respectively. The charge associated with both peaks (solid curve) was essentially identical and consistent with the presence of about $8 \cdot 10^{-11}$ moles/cm^2 of FeTsPc on the surface. This value is 2.6 times larger than that for FeTsPc adsorbed on the basal plane of HOPG [8]. If it is assumed that the average capacity of polycrystalline Ag in this solution is approximately 50 μF/cm^2, the value obtained from the dotted curve in Fig. 8 would correspond to a roughness factor of 3. This suggests that FeTsPc is adsorbed as a single monolayer on the Ag polycrystalline substrate.

The normalized reflectance spectra of FeTsPc adsorbed on the Ag surface (Fig. 6) obtained in sequence at 0.0, -0.3 and -0.4 V vs. SCE were found to exhibit features at 636 and 677 nm which compared very favorably with the solution-phase transmission spectrum for FeTsPc in the same electrolyte (see insert). The spectral feature was very similar to those reported for FeTsPc and CoTsPc on the Pt surface and the basal plane of HOPG by Nikolic et al. [9] who presented data at only one potential. These peaks at 636 and 677 nm have

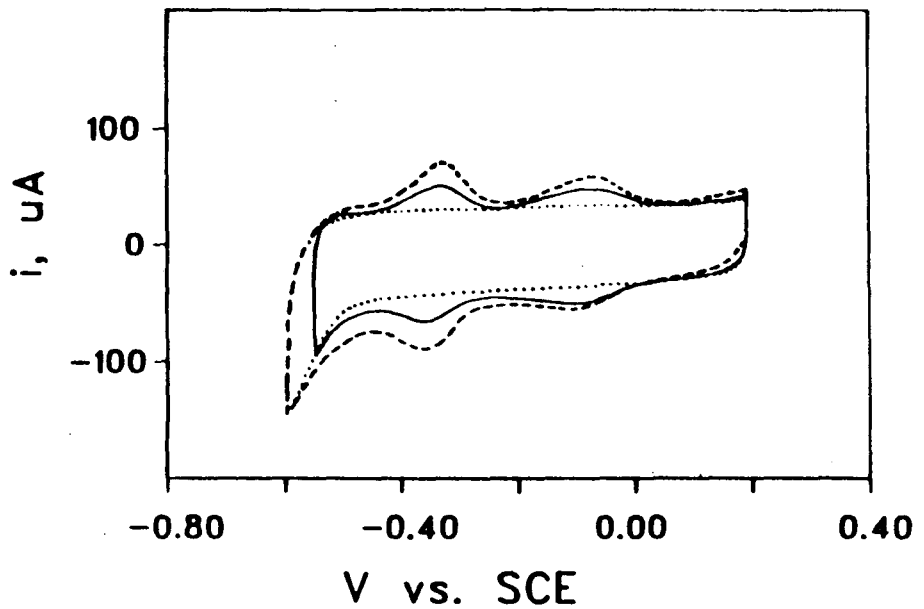

Fig. 5. Cyclic voltammograms of Ag in 0.05 M H_2SO_4;
dotted: bare Ag without adding FeTSPC,
dashed: in the presence of $1 \cdot 10^{-4}$ M FeTSTC, and
solid : with preadsorbed FeTSPC, no FeTSPC in solution.
A=2.6 cm^2, v=100 mV/s, $\Gamma = 8 \cdot 10^{-11}$ mole/cm^2.

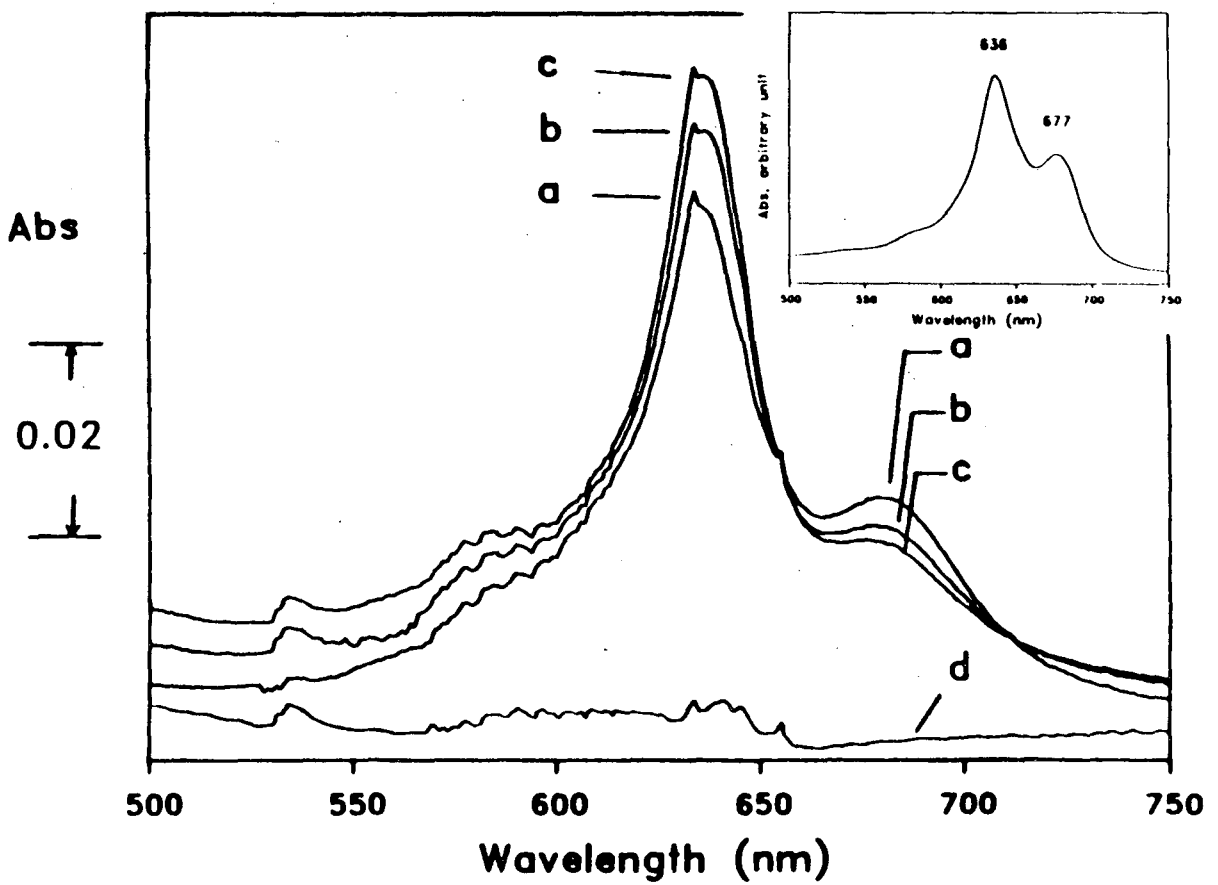

Fig. 6. *In-situ* Vis reflection spectra for FeTSPC adsorbed on Ag in 0.05 M H_2SO_4(no FeTSPC in solution); a: 0.0 V, b:-0.3 V, c:-0.4 V, d: 0.0 V after holding the potential at -0.5 V for 1 min.; normalized by the bare Ag spectrum; insert: CoTSPC solution transmission spectrum.

been assigned to the reduced and oxidized forms of the macrocycle, respectively. In particular, the oxidized species may involve oxygen-bound aggregates of the μ-oxo or μ-peroxo type, since the existence of oxygen in the solution was a prerequisite for FeTsPc adsorption on Ag as well as on HOPG. Based on the data presented, the longer wavelength peak seems to decrease at more negative potentials and does not increase in intensity in the proper sequence when the potential was stepped back to more positive value than -0.4 V. It is proposed that continuous polarization in the potential region examined leads to the gradual reduction of the oxidized form of μ-oxo FeTsPc to generate a monomeric species responsible for the shorter wavelength absorption peak at 636 nm. Evidence for a conversion between the two species is supported by the presence of a clear isobestic point at 650 nm. After these measurements were completed, the electrode was polarized at -0.5 V for one min. The obtained spectrum displayed no clear feature, which indicates that the original FeTsPc is either irreversibly desorbed or more probably destroyed by the exposure to such a reducing potential which is close to the hydrogen evolution potential. If FeTsPc desorbed from the surface and dispersed in the volume of the cell, it should be detected since the extinction coefficient of FeTsPc is $\sim 10^5$. This effect provides rather convincing evidence that the macrocycle detected by optical means is electrochemically active and the contribution from the material adsorbed on the prism window is negligible.

2. Voltammetric and FTIR Spectroscopic Examination of CoTMPP Adsorbed on Smooth Surfaces.

Fourier Transform infrared reflection-absorption spectroscopy (FTIRRAS) is known as a surface vibrational probe which has sensitivity to detect a monolayer of adsorbates on a conducting surface when a large incident angle and p-polarized radiation are employed, and a large number of interferometric scans

are averaged. Three FTIRRAS spectra of CoTMPP (1.5×10^{-10} moles/cm^2 or 10 monolayers) on Ag, Ni and HOPG were reported in last year's report [10]. The spectra for CoTMPP on Ag, Ni and HOPG were similar to each other and not much different from that of the bulk material.

When CoTMPP dissolved in acetone was injected into the electrochemical cell for HOPG, it revealed evidence for a strong interaction with the HOPG surface under potential control. Figure 7 shows the voltammograms of bare HOPG (dotted curve), the first cycle (dashed curve) and the steady state (solid curve) in the presence of CoTMPP ($\sim 10^{-5}$ M, total acetone in the electrolyte solution was less than 1%) in deaerated 0.05 M H_2SO_4. The first and the steady state curves were obtained after holding the potential at 0.0 V for 30 min. Clearly, there is a restructuring of CoTMPP during the potential cycling, and the restructured or reoriented molecules show reversible behavior in the cyclic voltammograms. The redox couple at 0.75 V shows a full width at half maximum (FWHM) of 80-90 mV which fits the theoretical shape expected for Langmuir-type behavior [11]. This CoTMPP restructuring did not occur until the positive potential limit reached 0.9 V. It is likely that Co(III) of the complex interacting with the surface is responsible for the apparent restructuring and the changes in the voltammetric curve in Fig. 7. A specific possibility is that the Co interacts through the axial ligand position with surface functional groups, residing on HOPG. The surface concentration could be very low since the CoTMPP molecule occupies a relatively large area. The interaction of Co with a surface group such as -C = O would increase the reversibility of charge transfer between the surface and the complex by a bridging mechanism. This might be related to the water-coordinated species [12].

Voltammetric measurements with variation of the CoTMPP solution concentration were attempted to examine the possibility of obtaining adsorption

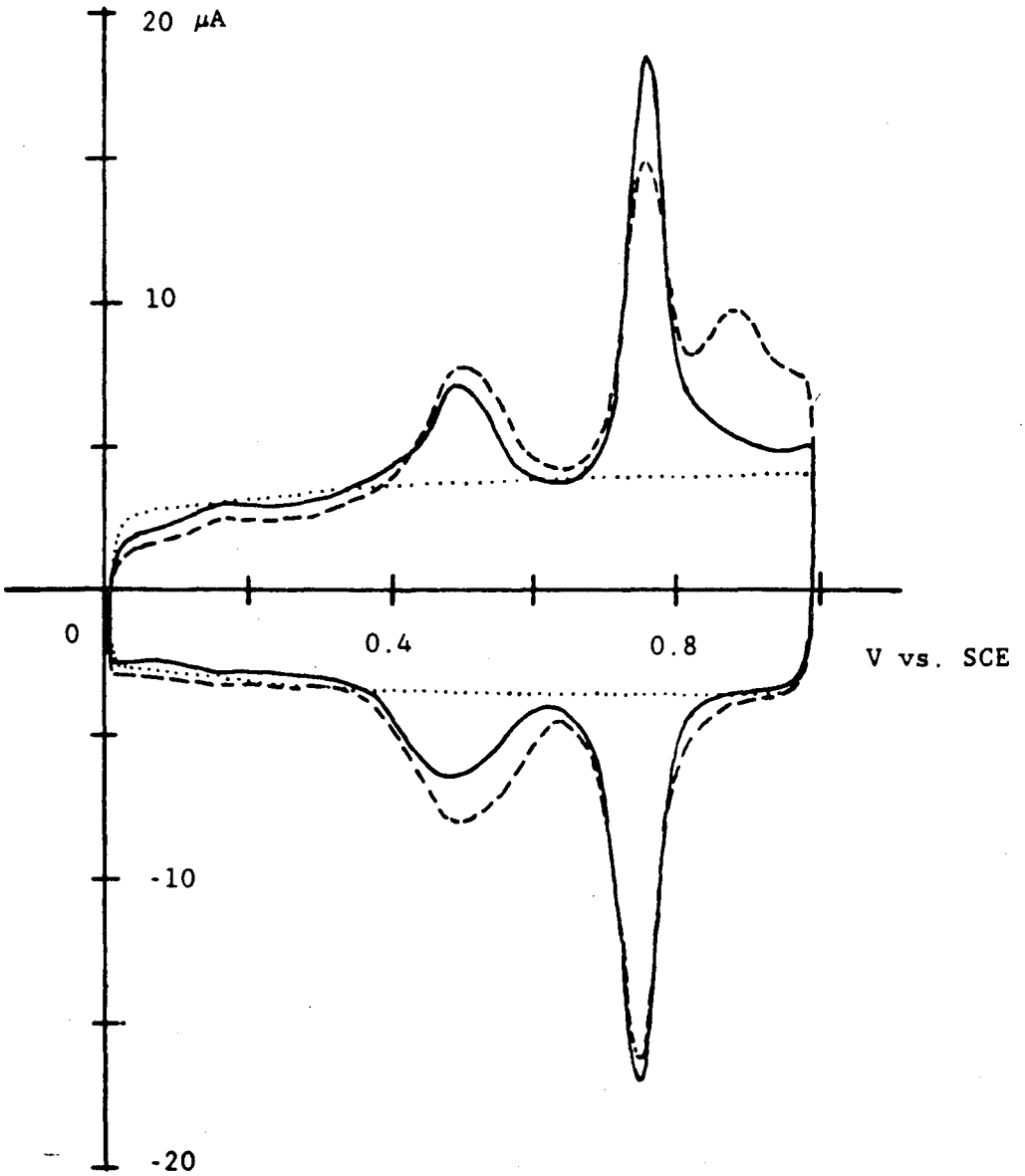

Fig. 7. Cyclic voltammograms for CoTMPP adsorbed on the basal plane of HOPG in 0.05 M H_2SO_4; CoTMPP/acetone was injected at 0.0 V vs. SCE to make the final concentration ~10^{-5} M. Dashed: the first cycle, solid: steady state, dotted: HOPG without CoTMPP; A=0.90 cm^2, v=500 mV/s, $\Gamma=1.8\cdot10^{-11}$ mol/cm^2. The voltammograms were taken 30 min after the injection.

isotherms. The result is given as a plot of the surface concentration vs. the solution concentration. The former was estimated from the voltammetric charge evaluated 30 min after injecting CoTMPP. Although the validity of the data is doubtful since adsorption on the cell wall is not negligible, the curve shape appears Langmuirian. A trial plot of $\theta/(1-\theta)$ vs. C_{CoTMPP} did not give a straight line. However, the saturation coverage of CoTMPP on the basal plane of HOPG was $1.8 \cdot 10^{-11} \sim 2.0 \cdot 10^{-11}$ moles/cm^2.

Three samples prepared by different methods were examined with FTIRRAS to gain insight into the orientation of CoTMPP molecules on the basal plane of HOPG. In Fig. 8, A shows the steady-state voltammogram for the sample obtained by acetone evaporation. B and C show those for layers measured by injecting the acetone solution into 0.1 M $HClO_4$ and 0.05 M H_2SO_4, respectively. The samples were thoroughly washed with pure water prior to the spectroscopic measurements. The spectra for these samples obtained by averaging 8000 interferometric scans (see the caption for the detail) are plotted in Fig. 9 and the preliminary assignments are given in Table II. The voltammogram A shows a irreversible Co(II)/Co(III) couple, which is probably the result of aggregation of CoTMPP formed during evaporation. The aggregated CoTMPP may have a slow charge transfer rate causing the peak displacement between the anodic and cathodic peaks. The potential difference of Co(II)/Co(III) peak between B and C may be because of anion effects or pH effects. The aggregation of CoTMPP in the case A is also evident in the spectrum A since all of the vibrational peaks for the bulk sample are seen unlike spectra B and C. Two common peaks were observed at 806 and 667 cm^{-1} in the three spectra, which correspond to C-H stretch and ring vibration of either benzene and pyrrole, respectively. Since the spectral features of A are not present in the spectra B and C, it is difficult to conclude as to the molecular orientation. The peaks associated

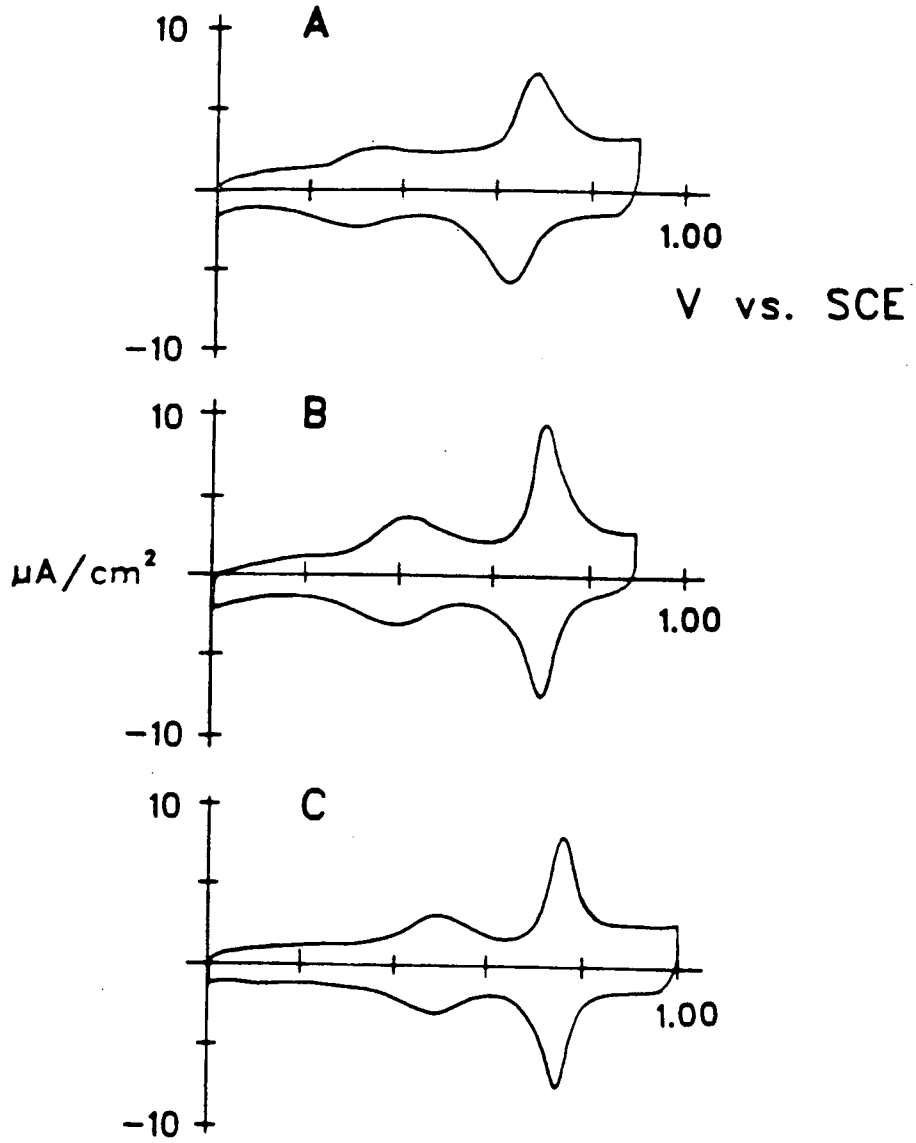

Fig. 8. **Cyclic voltammograms for CoTMPP adsorbed on HOPG by various methods A, acetone evaporation, in 0.05 M H_2SO_4; B, by injection of CoTMPP/acetone, in 0.1 M $HClO_4$; C, by injection of CoTMPP/acetone, in 0.05 M H_2SO_4. 200 mV/s, Γ=2.0-2.5·10^{-11} mole/cm^2, No CoTMPP in solution.**

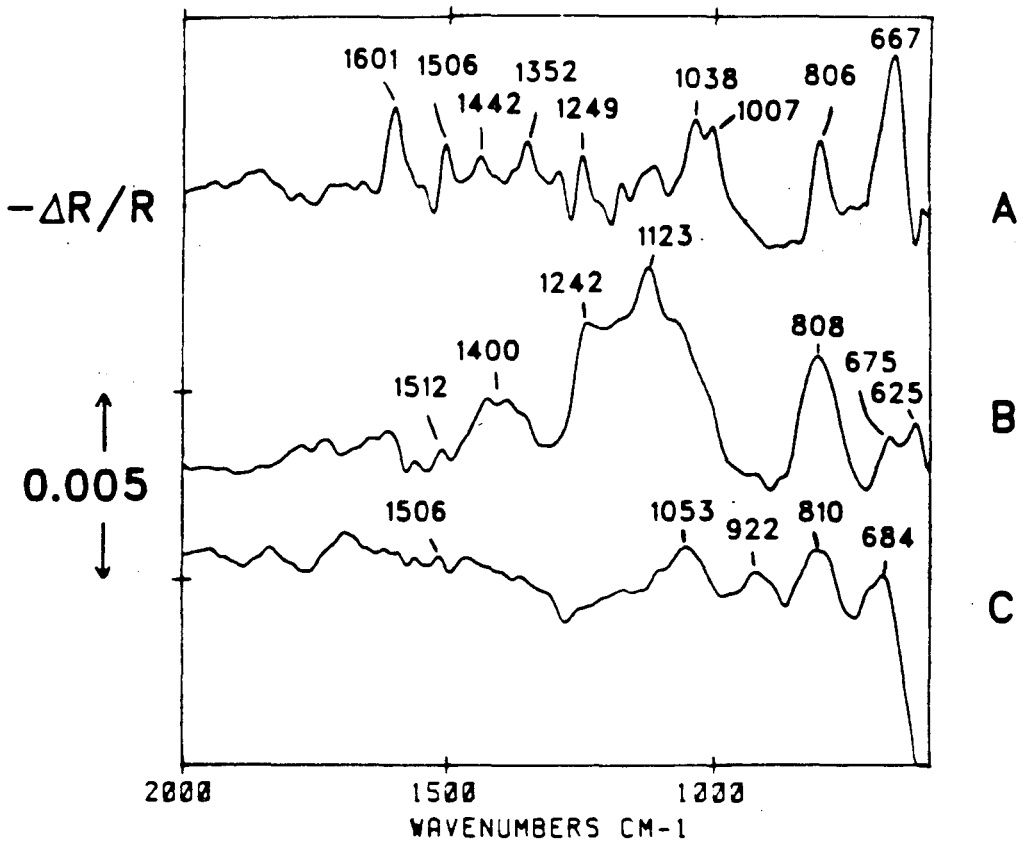

Fig. 9. Ex-situ FTIRRA spectra for CoTMPP adsorbed on HOPG by acetone evaporation(A), injection of CoTMPP/acetone in 0.1 M $HClO_4$(B) and injection of CoTMPP/acetone in 0.05 M H_2SO_4(C), 8000 scans, 75° incident angle, p-polarized. Normalized by the bare HOPG spectrum

TABLE II

Temporary assignments of peaks in FTIRRAS spectra for CoTMPP/HOPG

	cm^{-1}	modes	
spectrum A; [70]	1601	-C=C- stretch	
	1506	-C=C- stretch	
	1442	$-CH_3$ bending	
	1352	-C=N- stretch	
	1249	phenyl-C-O- stretch	
	1038	$-O-CH_3$ stretch	
	1007	pyrrole ring	
	806	benzene or pyrrole C-H	
	667	benzene or pyrrole ring	
spectrum B;	1123	ν_3	ClO_4^- [52]
	625	ν_4	
spectrum C;	1053	ν_3	SO_4^{2-} [52]
	922	ν_1	

with perchlorate and sulfate anions are seen in B and C, respectively (see also Table II).

If CoTMPP molecules are adsorbed parallel to the basal plane of HOPG, the two peaks at 806 and 667 cm^{-1} can be explained since the peripheral phenyl group is perpendicular to the molecular plane as a result of the repulsion between the phenyl hydrogen and pyrrole hydrogen. However, the -C=C- stretches of the phenyl group are not present at ~1600 cm^{-1} but only at 1506 and 1512 cm^{-1} in spectra B and C. On the basis of that, the restructuring of CoTMPP on HOPG is directly related to Co(III) and most of the fine structures in the IR spectrum for the bulk CoTMPP do not appear in the surface spectra. It is proposed that CoTMPP is anchored parallel to the HOPG surface when it is adsorbed from the electrolyte solutions by potential cycling.

The Raman data for $(FeTMPP)_2O$ reported by Holze were interpreted to propose a perpendicular orientation of this molecule [13]. However, this is for the μ-oxo structure of $(FeTMPP)_2O$. Moreover, Holze prepared his sample by evaporation, which gives an ill-defined layer as proven in our results. Since evaporation gives a random orientation as shown in Fig. 9A, the bands corresponding to perpendicularly oriented molecules become relatively pronounced in the spectra.

CoTMPP molecules are also strongly adsorbed on Pt electrodes. After obtaining a clean Pt voltammogram in 0.05 M H_2SO_4, CoTMPP/acetone was injected at open- circuit conditions to make the final concentration ~10^{-5} M in the electrolyte solution. The voltammogram was featureless as shown by the dashed curve in Fig. 10. It indicates that CoTMPP is probably adsorbed as a multilayer on Pt, and this layer is a very poor conductor and blocks electrolyte from penetrating through. However, when oxygen was purged through the solution, a large O_2 reduction current was observed. It is not clear whether this is for O_2 penetration through the hydrophobic CoTMPP matrix [14] (so called *dry*

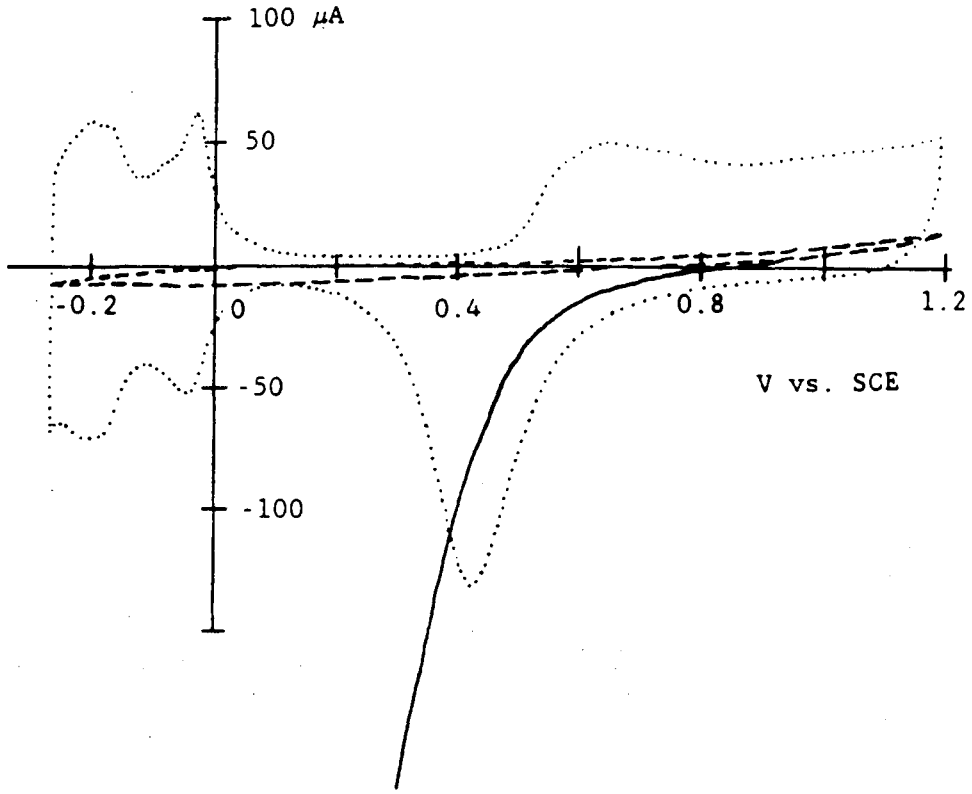

Fig. 10. Cyclic voltammograms CoTMPP adsorbed on Pt in 0.05 M H_2SO_4; CoTMPP/acetone was injected to give ~10^{-5} M at open circuit conditions; dotted: bare Pt, dashed: with CoTMPP, solid: after O_2 saturation; 100 mV/s, A=0.3 cm^2.

cave effect [15]) or O_2 reduction at the outer plane of CoTMPP layer. The hydrogen adsorption feature appeared slowly with continuous potential cycling involving O_2 reduction, which indicates damage of the CoTMPP layer probably due to the reaction with either peroxide or superoxide ions generated during O_2 reduction.

With the introduction of O_2, the CoTMPP film appears to become conducting as the potential is scanned into the region where Co(II) becomes stable (Fig. 10). The O_2 is probably reduced to O_2^- and resides between the planes of the CoTMPP layers. Thus the conduction proceeds as follows:

```
Co(II)   Co(II)   Co(II)   Co(III)   +   O2
                           |
                           O2-

Co(II)   Co(II)   Co(II)   Co(II)

Co(II)   Co(II)   Co(II)   Co(II)

                     O2-
                     |
Co(II)   Co(II)   Co(III)  Co(II)
```

Since most of oxygen adducts of cobalt macrocycles reported are superoxide-like species [14], this mechanism for O_2 penetration and electrical conductivity is reasonable.

3. <u>In-situ</u> FTIRRAS Studies of FeTsPc on Ag and OPG Electrodes

<u>In-situ</u> FTIRRAS spectra were also obtained for FeTsPc adsorbed at monolayer coverages on Ag and OPG electrodes in 0.1 <u>M</u> $HClO_4$ solution by a CWRU-built reflection-absorption optics with p-polarization at 70° incident angle [17] and an IBM-98 FTIR spectrometer [12].

FeTsPc was adsorbed from 1 x 10^{-5} <u>M</u> FeTsPc in 0.1 <u>M</u> $HClO_4$ solution in the spectro-electrochemical cell [17] by cycling the potential between -0.50 V and +0.15V vs. SCE for the Ag electrode and between -0.50 V and +0.70 V vs. SCE for

the OPG electrode respectively. Prior to the spectroscopic measurements, the solution-phase FeTsPc was removed by flushing the cell with a fresh 0.1 M $HClO_4$ solution. The infrared spectra were obtained at various potentials relative to the spectrum at 0.0 V vs. SCE as the reference state.

The preliminary spectra for both Ag and OPG electrodes were basically identical except for the poor S/N ratio with the OPG electrode because of the poor surface reflectivity. A weak band at 1627 cm^{-1} was observed over the potential range -0.2 to -0.4 V and there were no spectral features in the spectral range, 1300 - 1600 cm^{-1} where C = N and C = C stretching of the TsPc ligand backbone are located (Fig. 11). The peak at 1027 cm^{-1} was assigned to asymetric S-O stretching of sulfonate group in the *ex-situ* data reported by Bae [12]. One explanation is that the macrocycle may be oriented edge on and only the sulfonic acid groups undergo significant vibrational change with the electric field in the interface. Consequently the other vibrational modes of the ligand are unchanged in the adsorbed state. However, more work is needed to confirm this.

C. Controlled Poisoning of Transition Metal Macrocycles

In order to obtain further insight concerning the redox properties and O_2 reduction electrocatalysis on transition metal macrocycles, the effect of CN^-, capable of coordinating with the transition metal in the axial position, has been examined. The interaction of the CN^- ions with the transition metal of the macrocycle can affect the intrinsic electrochemical behavior, and the CN^- adduct can undergo redox reactions. The major focus, however, has been on the competitive interaction of CN^- and O_2 with the transition metal in the axial position and the effect on O_2 reduction. These studies were carried out with Fe-TsPc and Co-TsPc preadsorbed in monolayer coverages on ordinary pyrolytic graphite (OPG) rotating disk electrode as well as non-heat-treated and heat-treated tetramethoxy phenyl porphyrins (TMPP) on Vulcan XC-72 carbon in the

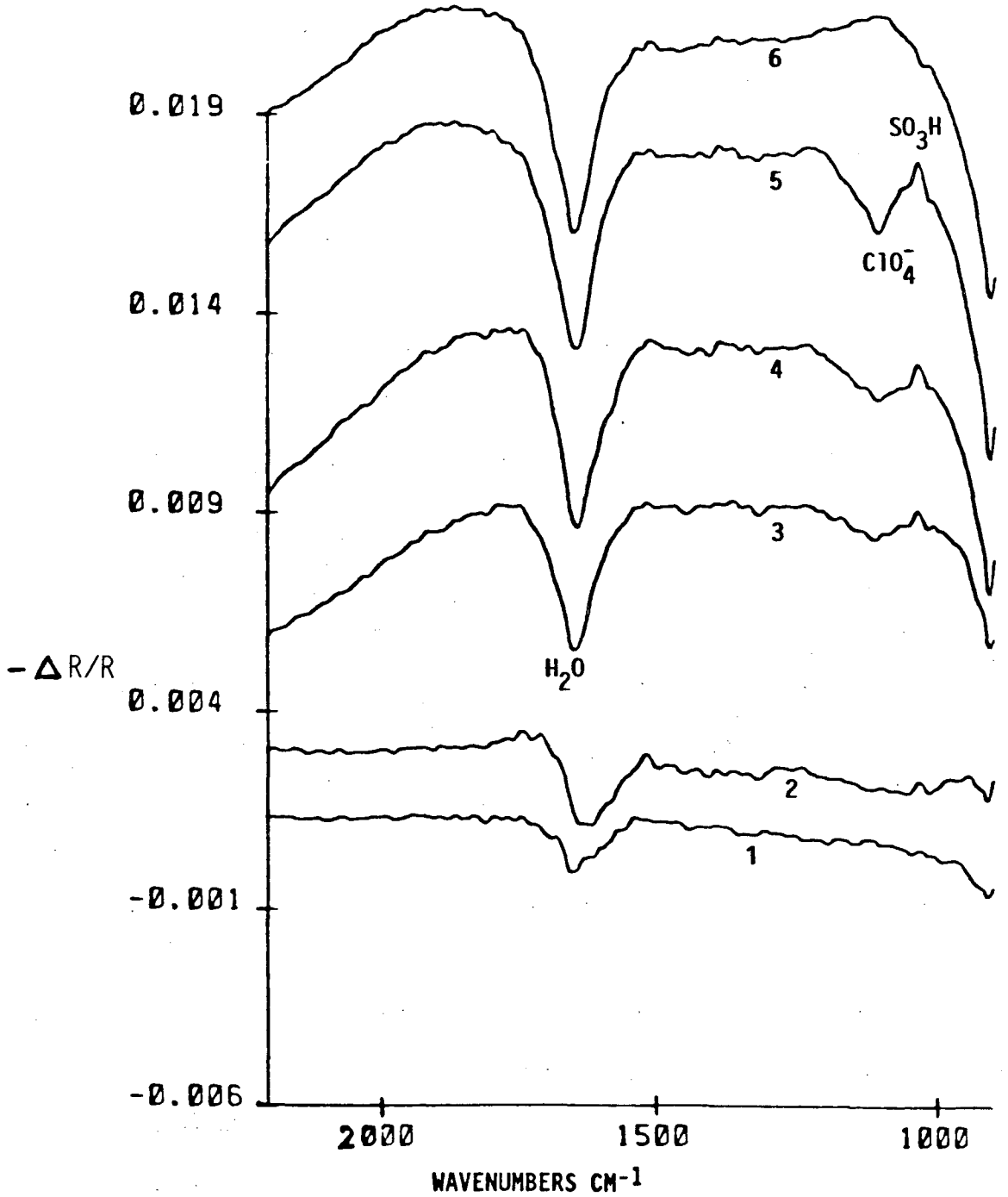

Fig. 11. In-situ Fourier transform infrared reflection absorption (FTIRRA) spectra of monolayer adsorbed FeTsPc on Ag in 0.1 M $HClO_4$ at fixed potentials. P-polarized light. Angle of incidence = 70°. E (V) vs. SCE.

1.	-0.1 V	4.	-0.4 V
2.	-0.2 V	5.	-0.5 V
3.	-0.3 V	6.	+0.15 V

form of a thin porous coating (TPC) layer on an OPG rotating disk with Teflon as the binder in 0.1 M NaOH solutions.

1. Fe- and Co-TsPC

Figure 12 shows that Fe(III) and Fe(II) in FeTsPc can bind CN^- in the axial position, thus hindering their redox processes and significantly inhibiting O_2 reduction kinetics (Fig. 13). O_2 is reduced by a 2-electron process on FeTsPc in the presence of CN^- (~1 x 10^{-3} M) whereas in the absence of CN^- it is reduced by a 4-electron process [18] at low cathodic potentials. In the presence of CN^-, the axial positions are blocked and O_2 reduction probably occurs principally on the OPG substrate. Reduction of the TsPc ligand (Peak 1), as mentioned earlier [19], is influenced to a minor extent by the presence of CN^- ions. However, peak 4 [19, 20] [the assignment of Fe(IV)/Fe(III) or TsPc ligand oxidation] is affected only to a small extent with CN^- in solution (Fig. 14), indicative that this peak corresponds to oxidation of the ligand. This conclusion is further confirmed from voltammetry of H_2TsPc in the same solution. The presence of CN^- results in a new anodic and complementary cathodic peak in the voltammetry curve (Fig. 14). These peaks are irreversible and insensitive to agitation of the solution and appears to be associated with CN^- coordinated to the adsorbed Fe in FeTsPc.

Co(II) (d^7) in CoTsPc does not bind CN^- axially, in analogy with the isoelectronic Fe(I) (d^7) [21] (see Fig. 15). Therefore there is no significant inhibition effect of CN^- on the reduction of O_2. The amplitude of the ligand (TsPc) reduction peak is decreased to a small extent. Peak 3 [19, 20] in the voltammogram of CoTsPc in 0.1 M NaOH is confirmed to correspond to Co(III)/Co(II). This peak shifts by about 345 mV in the negative direction in the presence of CN^- (Fig. 15), as expected since Co(III) binds CN^- in its axial position.

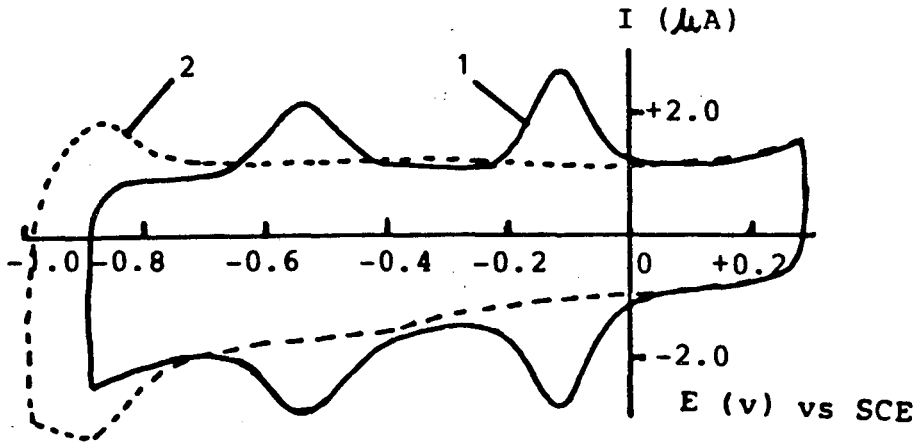

Fig. 12. Cyclic voltammograms (Peaks 2, 3) of FeTsPc adsorbed on OPG in 0.1 M NaOH (Ar satd.) without and with 1×10^{-3} M CN^- in solution. Disk area = 0.2 cm^2. Scan rate = 150 mV/s.

1 - without CN^-
2 - with 1×10^{-3} M CN^-

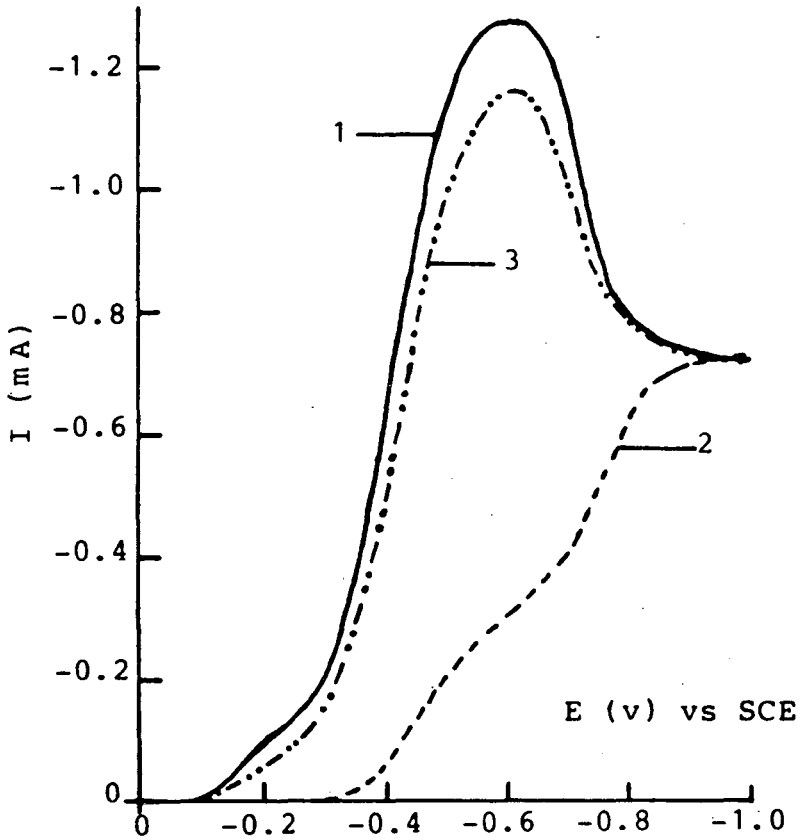

Fig. 13. Polarization curves for O_2 reduction (1 atm) on FeTsPc adsorbed on OPG in 0.1 M NaOH without and with 1 x 10^{-3} M CN^- in solution. Disk area = 0.2 cm^2. Scan rate = 10 mV/s; 2500 rpm.

1 - without CN^-
2 - with 1 x 10^{-3} M CN^-
3 - electrode after 2, washed and diped in fresh 0.1 M NaOH.

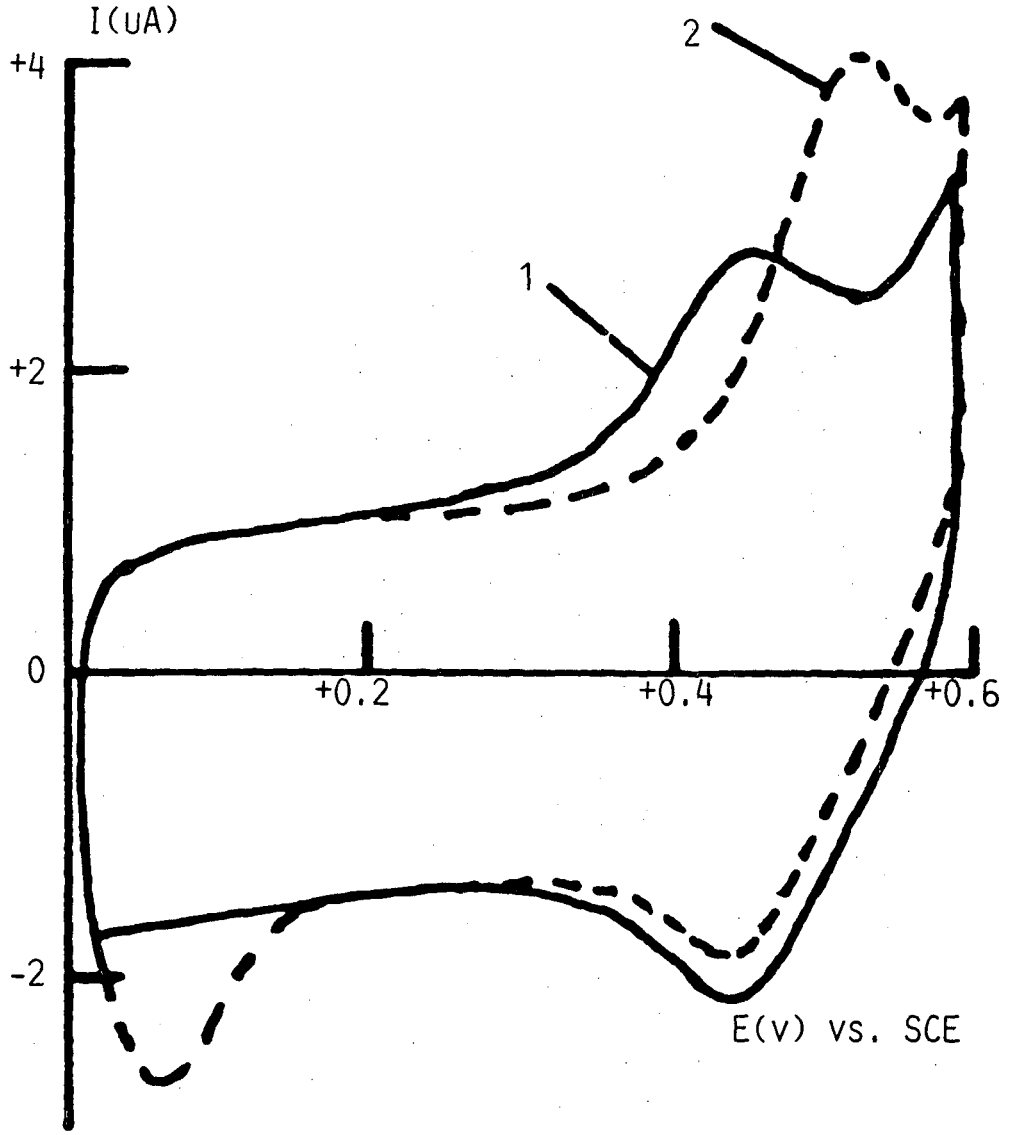

Fig. 14. Cyclic voltammogram (peak 4) of FeTsPc adsorbed on OPG in 0.1 M NaOH (Ar satd.) without and with 5×10^{-3} M CN^- in solution. Scan rate = 150 mV/s. Disk area = 0.2 cm^2.

1 - without CN^-
2 - with 5×10^{-3} M CN^-

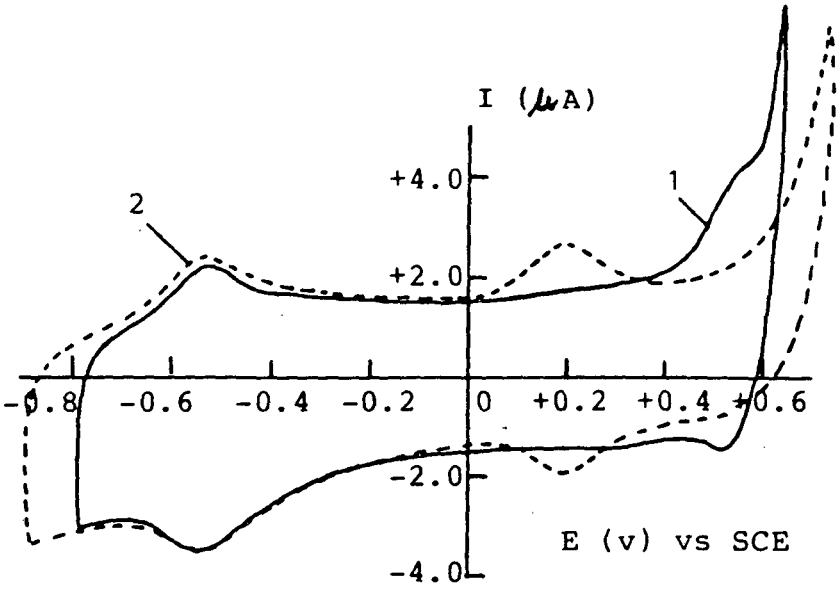

Fig. 15. Cyclic voltammograms (Peaks 2, 3) of CoTsPc adsorbed on OPG in 0.1 M NaOH (Ar satd.) without and with 2 x 10^{-3} M CN^- in solution. Disk area = 0.2 cm^2. Scan rate = 150 mV/s.

1 - without CN^-
2 - with 2 x 10^{-3} M CN^-

2. Fe- and Co-TMPP

As expected, there is practically no effect of CN^- (~1 x 10^3 M) on the redox behavior of the Fe(III)/Fe(II) couple [22] in the non-heat-treated μ-oxo $(FeTMPP)_2O$ on Vulcan XC-72 (Fig. 16). Oxygen is strongly bound axially between two irons in the μ-uxo bridged dimer [Fe-O-Fe] in this complex and is not displaced by CN^-. Therefore, there is practically no inhibition of O_2 reduction on the non-heat-treated $(FeTMPP)_2O$/XC-72 by the presence of CN^- in solution. In the absence of CN^-, the voltammogram of the heat-treated (800 °C) $(FeTMPP)_2O$/XC-72 gives no peak for the Fe(III)/Fe(II) couple, but shows a small irreversible cathodic and anodic peak involving $FeOOH/Fe(OH)_2$ in alkaline solution, particularly when the electrode is exposed to more cathodic potentials (~ -1.3V vs. SCE) [22]. However, this peak is eliminated in the presence of ~5 x 10^{-3} M CN^- in 0.1 M NaOH after potential cycling between +0.2 to -1.3 V vs. SCE for about 1 h.

The half-wave potential for O_2 reduction on heat-treated $(FeTMPP)_2O$/XC-72 is shifted by ~75 mV more cathodic in the presence of CN^- as compared to that without CN^- in solution. However, the same electrode regains activity for O_2 reduction when it is dipped in fresh O_2-saturated 0.1 M NaOH without CN^-. This indicates that $(FeTMPP)_2O$ is decomposed during heat treatment. In the presence of CN^-, the axial positions are blocked and O_2 reduction probably occurs principally on Vulcan XC-72.

The redox couple Co(III)/Co(II) [22] in non-heat-treated CoTMPP/XC-72 shifts by ~500 mV more negative in the presence of CN^- (Fig. 17). The voltammogram of the heat-treated CoTMPP/XC-72 (800°C) does not give a Co(III)/Co(II) peak but shows a small oxidation peak for $Co(OH)_2$ in 0.1 M NaOH [22]. However, this peak disappears when CN^- is present in solution. O_2 reduction on CoTMPP/XC-72 is significantly inhibited by -60 mV with and by -120 mV without heat-treatment by CN^- (Fig. 18). Inhibition is greater with the

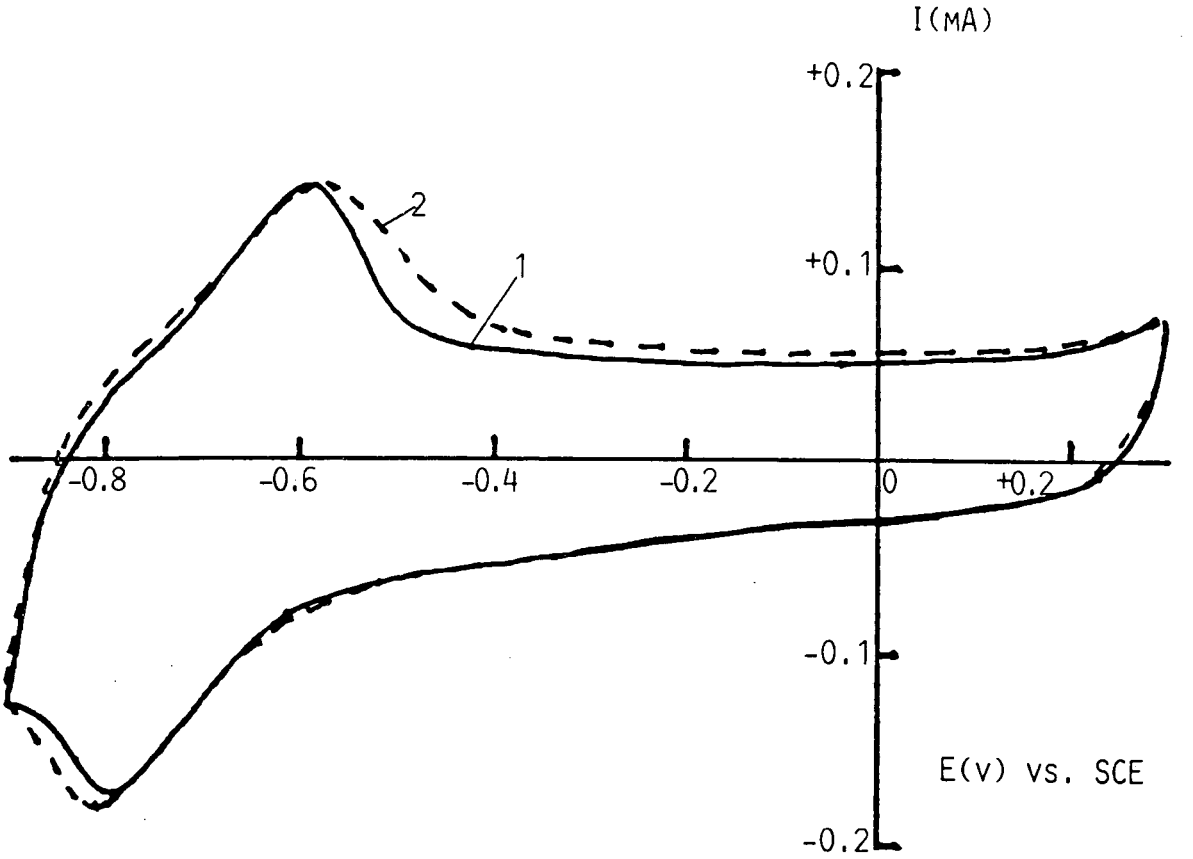

Fig. 16. Cyclic voltammogram of 5% $(FeTMPP)_2O$/XC-72 (non-heat-treated) in the form of TPC electrode in 0.1 M NaOH (Ar satd.) without and with 1 x 10^{-3} M CN^- in solution. Electrode area, geometrical = 0.2 cm^2. Scan rate = 20 mV/s. Teflon = 10%.

1 - without CN^-
2 - with 1 x 10^{-3} M CN^-

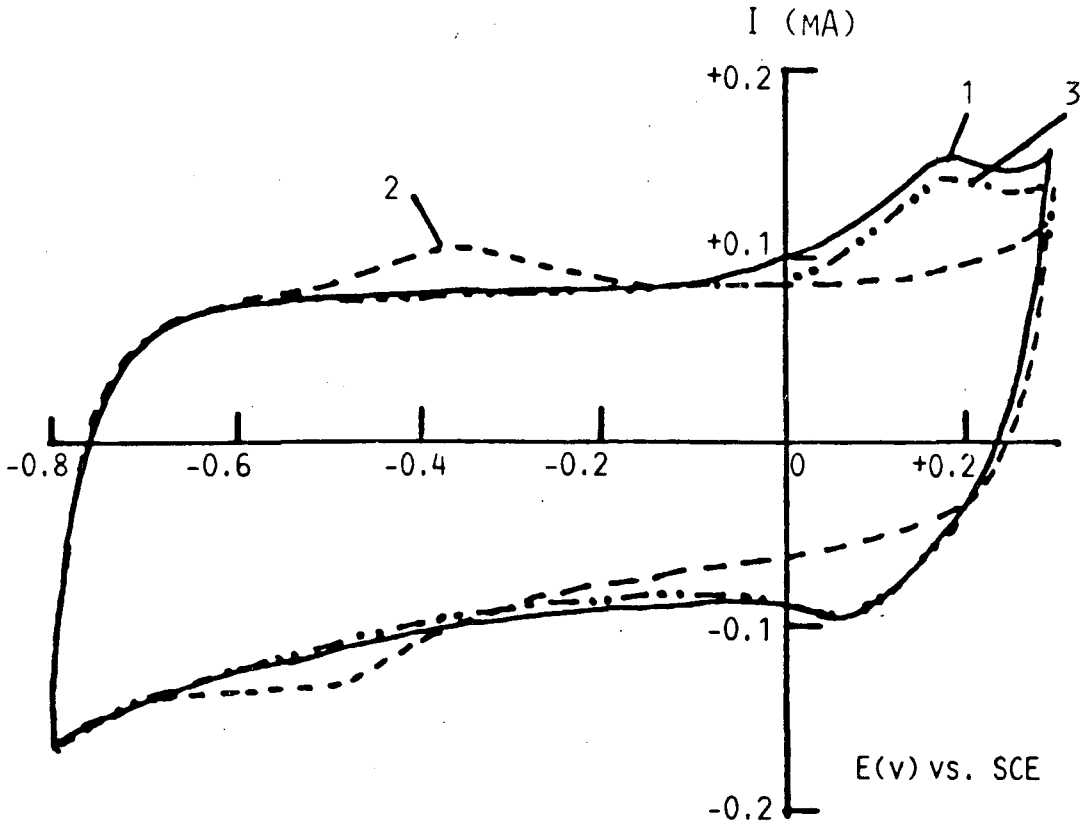

Fig. 17. Cyclic voltammogram of 5% CoTMPP/XC-72 (without HT) in the form of TPC electrode in 0.1 M NaOH (Ar satd.) without and with 1×10^{-3} M CN^- in solution. Electrode area, geometrical = 0.2 cm^2. Scan rate = 20 mV/s. Teflon 10%.

1 - Without CN^-
2 - with 1×10^{-3} M CN^-
3 - Electrode after 2, washed and dipped in fresh 0.1 M NaOH (Ar satd.) without CN^-.

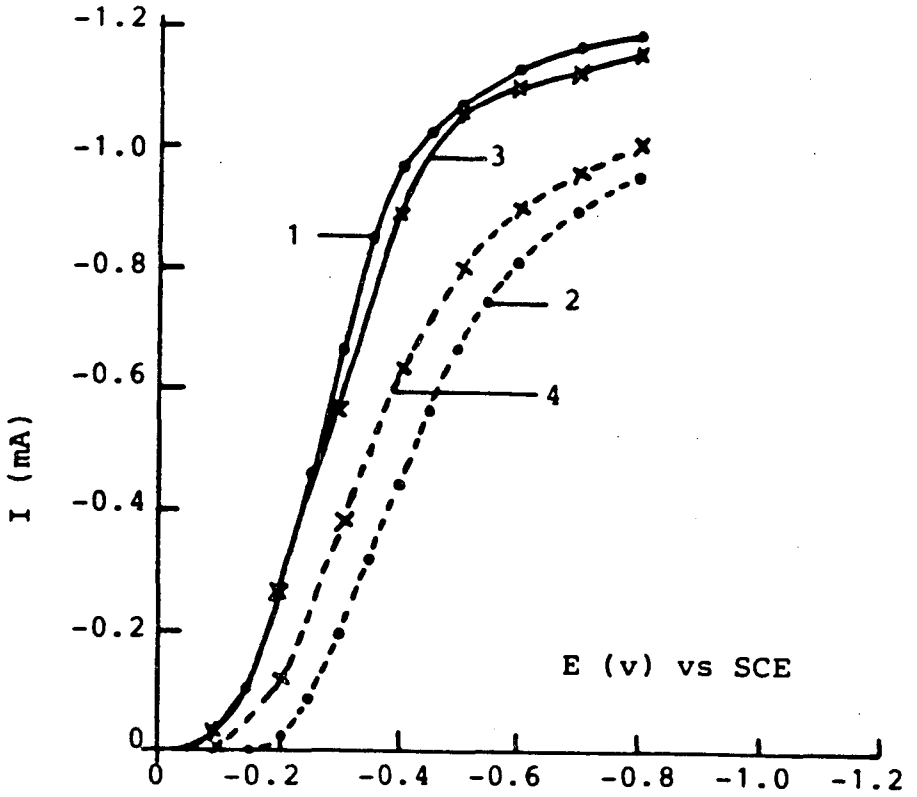

Fig. 18. Polarization curves for O_2 reduction (1 atm) on 5% CoTMPP/XC-72 without and with heat treatment (800°C) in 0.1 M NaOH without and with 5 x 10^{-3} M CN^- in solution. Rotation rate = 2500 rpm. Point by point curves in cathodic direction. Electrode area, geometrical = o.2 cm^2.

1 - CoTMPP/XC-72 (No HT) without CN^- in 0.1 M NaOH
2 - CoTMPP/XC-72 (No HT) with 5 x 10^{-3} M CN^- in 0.1 M NaOH
3 - CoTMPP/XC-72 (800°C HT) without CN^- in 0.1 M NaOH
4 - CoTMPP/XC-72 (800°C HT) with 5 x 10^{-3} M CN^- in 0.1 M NaOH

non-heat-treated sample as compared to heat-treated CoTMPP/XC-72 in the presence of the same amount of CN^- in solution. The decrease in inhibition by CN^- for O_2 reduction with heat-treated CoTMPP/XC-72 as compared to the non-heat-treated material may be, to some extent, due to less blocking axially by CN^- as a result of partial decomposition of the ligand and other structural changes in the molecule after heat treatment.

These results confirm that a strong axial interaction of O_2 with the transition metal is an important factor in O_2 electrocatalysis. This study has also helped in confirming the redox processes associated with the voltammetric peaks obtained with transition-metal macrocycles.

D. Pyrochlore Electrocatalysts

1. Synthesis

Metallic oxides with the pyrochlore structure have attracted attention in recent years for their high catalytic activity both for O_2 reduction and generation [25-29]. A series of pyrochlores described by the general formula $Pb_2[Ru_{2-x}Pb_x]O_{6.5}$ where x = 0, 0.2, 0.3, 0.4, 0.6, 0.8 and 1.0 was synthesized at CWRU following the method of Horowitz et al. [28] (see Table III). The samples were characterized by X-ray diffraction and XPS.

2. X-ray diffraction and XPS studies

The ruthenium pyrochlore $Pb_2Ru_2O_{6.5}$ continues to be of interest for bifunctional O_2 electrodes in alkaline solution. This pyrochlore, heat-synthesized at 100°C, was further heat-treated between 300° and 500°C in flowing air and characterized by X-ray diffraction and XPS. No shift in the Ru, Pb or oxygen peaks was detected in the XPS spectra. X-ray diffraction of $Pb_2Ru_2O_{6.5}$ powder synthesized at 100°C showed broad peaks while the peaks became sharp after the pyrochlore was heated at higher temperatures.

3. TGA studies

TABLE III

Pyrochlores Used in the CWRU Research
on O_2 Reduction and Generation

No.	Compound	Preparation Method	XRD	Surf. Area $m^2\ g^{-1}$
1	$Pb_2Ru_2O_{6.5}$	(Exxon)	sharp	2
2	$Pb_2[Ru_{1.67}Pb_{0.33}]O_{6.5}$	(Exxon)	broad	55
3	$Pb_2Ru_2O_{6.5}$	hydrox. ppt., NH_3, 350°C HT	sharp	6
4	$Pb_2Ru_{1.5}Ir_{0.5}O_{7-y}$	O_2 sat. sol. phase, 4M KOH	broad	-
5	$Pb_2[Ru_{1.8}Pb_{0.2}]O_{6.5}$	O_2 sat. sol. phase, 4M KOH 100°C	broad	-
6	$Pb_2[Ru_{1.0}Pb_{1.0}]O_{6.5}$	O_2 sat. sol. phase, 4M KOH	broad	-
7	$Pb_{1.5}Co_{0.5}Ru_2O_{7-y}$	nitrate decomp., 750°C	sharp	-
8	$Y_2Ru_2O_7$	nitrate decomp., 750°C	sharp	-
9	$Dy_2Ru_2O_7$	nitrate decomp., 750°C	sharp	-
10	$Pb_2Ru_2O_{6.5}$	O_2 sat. sol. phase, 4M KOH, 75°C	broad	35
11	$Bi_{1.5}Co_{0.5}RuIrO_{7-y}$	nitrate decomp., 950°C	sharp	-
12	$Pb_2Ru_{1.2}Ir_{0.8}O_{7-y}$	O_2 sat. sol. phase, 4M KOH, 100°C	broad	-

Thermal gravimetric analysis (TGA) of $Pb_2Ru_2O_{6.5}$ was done under O_2 purge and also under N_2 purge. In both sets of measurements a weight loss of 3 to 3.5% was detected for temperatures from 100 to 900°C at a scan rate of 15 °C/min (Fig. 19). Upon maintaining the temperature at 800°C for an additional 2 h in O_2, no further weight loss was observed with the sample held at 800°C. Most likely the weight loss was due to the loss of chemically bound water in the pyrochlore.

4. Peroxide decomposition

Rate constants of peroxide decomposition were obtained by monitoring its concentration change at a rotating Au disk electrode. The peroxide concentration ($C_{HO_2^-}$) was monitored by measuring the diffusion limiting current for peroxide oxidation ($HO_2^- + OH^- \longrightarrow O_2 + H_2O + 2\ e^-$) on a Au disk electrode (area = 0.4 cm^2). A known amount of pyrochlore powder (5 to 30 mg) was dispersed in 70 ml of a N_2-saturated solution of 1 M KOH. Typically, 1.0 ml of 0.1 M H_2O_2 (reagent grade) was added to the solution and ($C_{HO_2^-}$) was monitored as a function of time (t). Before every measurement, the Au disk electrode was polarized at -1.0 V vs. Hg/Hgo, OH^- for 3 min to remove the oxide layer on Au.

The apparent rate constant, $k'\ s^{-1}$ was determined from the slope of the plot log i_l vs t (Fig. 20). It was found that k' is directly proportional to the weight of the dispersed catalyst and follows the equation $d[H_2O_2]/dt = k_w (w/V)[H_2O_2]$ where k_w(ml $g^{-1}s^{-1}$) is the rate constant per gram of catalyst in one ml of solution. The values of k_w and the heterogenous rate constant k_s, per m^2 of the catalyst surface area (from BET measurements) were calculated.

The effect of $[OH^-]$ concentration on H_2O_2 decomposition by $Pb_2Ru_2O_{6.5}$ was also studied by using 0.1 M to 4.0 M KOH solutions (Fig. 21). It was found that the rate of peroxide decomposition decreases as the concentration of $[OH^-]$

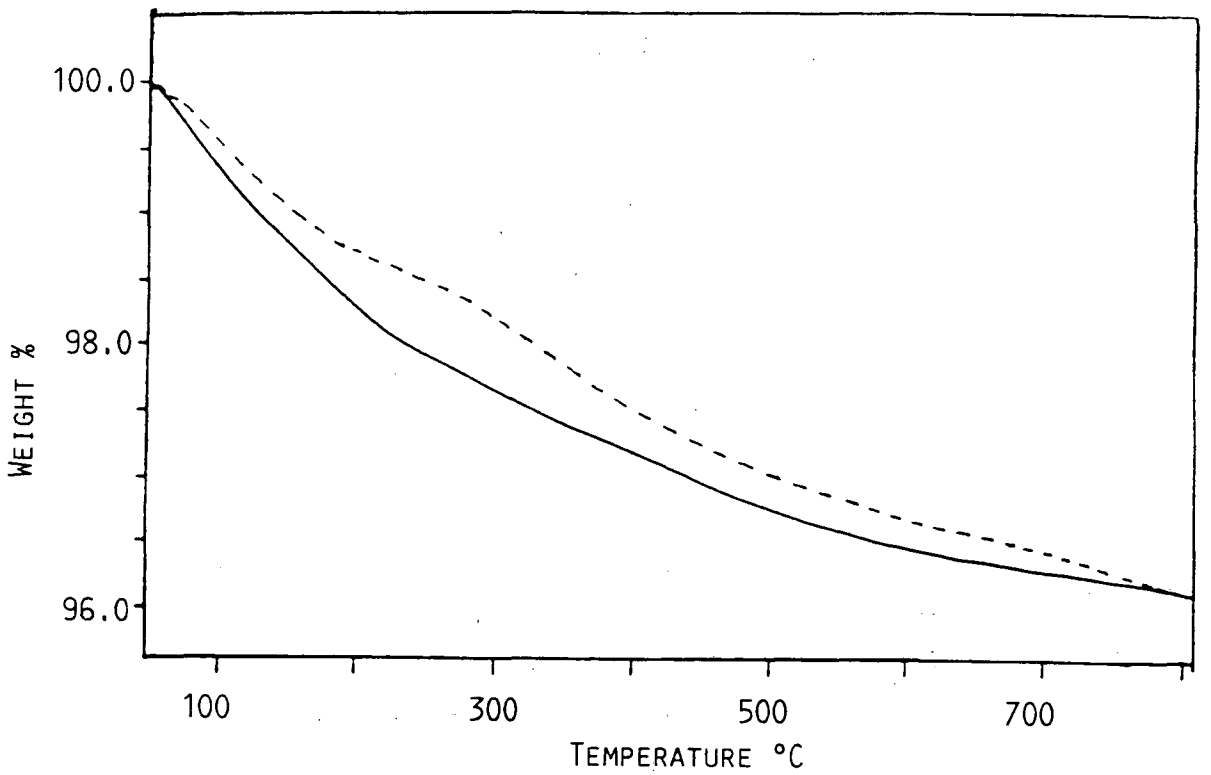

Fig. 19. Thermal gravimetric analysis of $Pb_2Ru_2O_{6.5}$ synthesized at 100°C. Solid line: N_2 purge, temperature scan rate: 10°C/min. Dashed line: O_2 purge, temperature scan rate: 15°C/min.

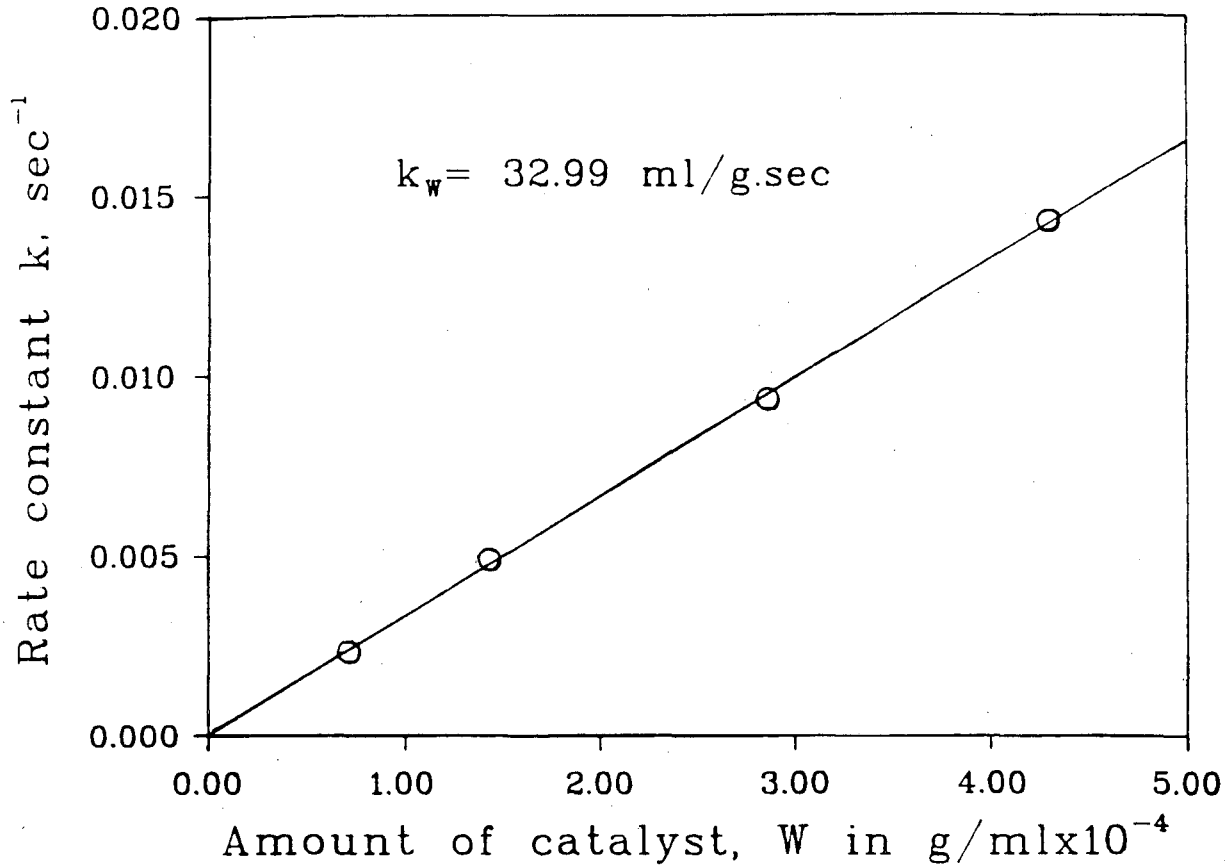

Fig. 20. Apparent first order rate constant for peroxide decomposition vs. amount of catalyst in 1 M KOH, initial concentration of hydrogen peroxide = 10^{-2} M.

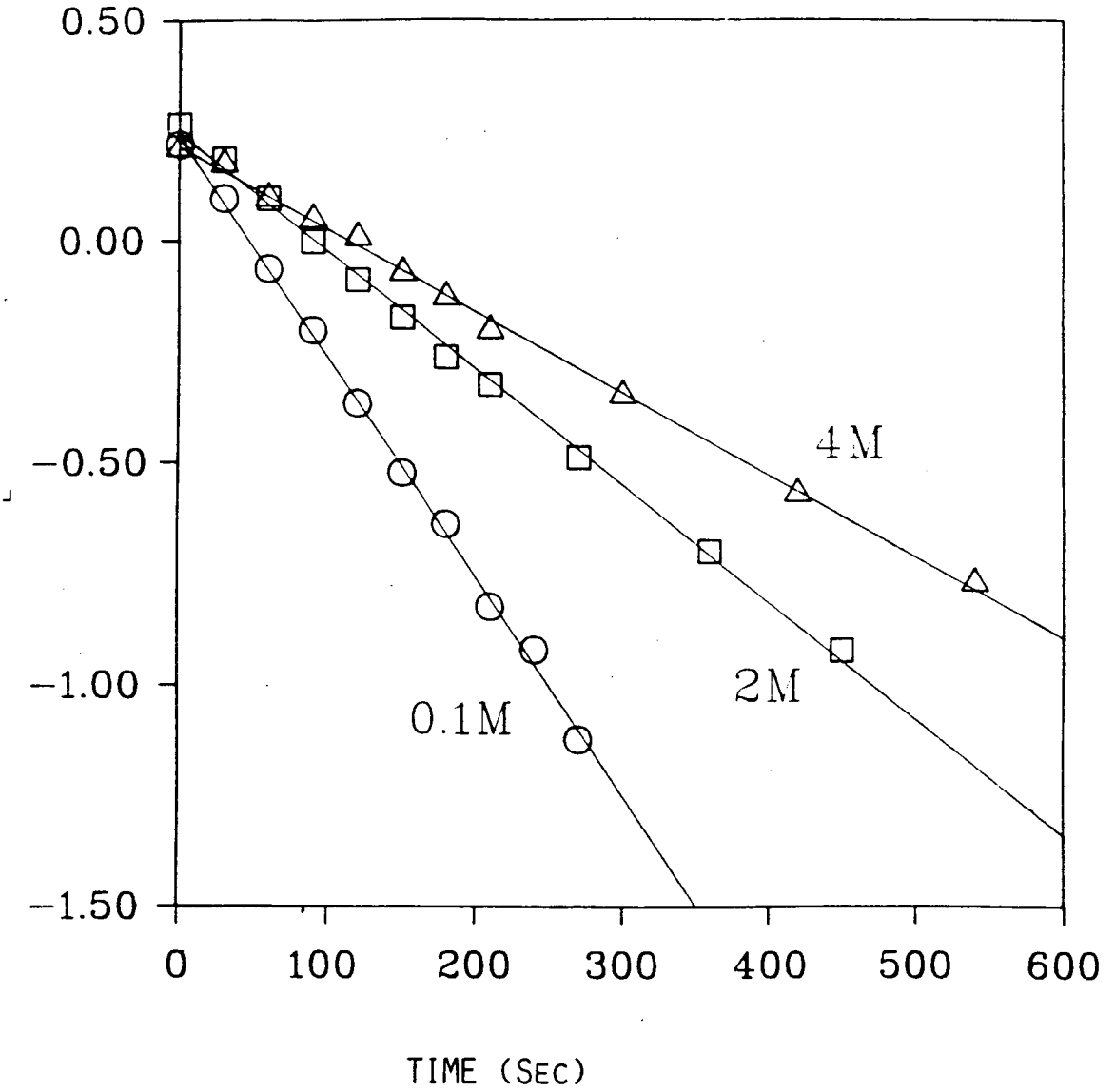

Fig. 21. Effect of KOH concentration on hydrogen peroxide decomposition kinetics with $Pb_2Ru_2O_{6.5}$. Catalyst concentration: 5 mg in 70 ml of KOH. Initial hydrogen peroxide concentration = 10^{-2} M.

increases. A plot of log k_w vs. $[OH^-]$ follows the equation log k_w = log a - $b/2.3[OH^-]^{1/2}$, (a an b are constants), with some scatter of the data particularly at 1 M KOH. The interpretation of the dependence of the heterogeneous rate constant with $[OH^-]$ is under investigation.

E. Heat-treated Polymeric Phthalocyanine and Pyrochlore Catalysts

1. Heat-treated polymeric phthalocyanine catalysts

Heat-treated transition-metal macrocycles such as Fe- and Co-TMPPP and Co-TAA dispersed on high-area carbons showed high activity and stability for O_2 reduction in alkaline and acid electrolytes. During the past year, the effect of heat-treatment of the sheet-type polymeric Fe- and Co-Pc adsorbed on Vulcan XC-72 carbon for O_2 reduction was investigated. These materials were heat-treated in a horizontal tube furnace at 400°C and 850°C under continuous flow of purified argon (Matheson, HP grade) for two hours and allowed to cool while still under flowing argon. A thin-porous-coated (TPC) electrode technique [23] was used for the voltammetric and O_2 reduction polarization studies in 0.1 M NaOH at room temperature, while porous gas-fed electrodes were used for polarization measurements in 4 M NaOH at 60°C [24].

The voltammetric curves for the non-heat-treated and the heat-treated polymeric FePc were obtained. The voltammogram is featureless for the material which has been heat-treated even at 400°C, although the catalytic activity of O_2 reduction is very similar to the non-heat-treated material (Fig. 22). Heat treatment to 850°C produces a material which is considerably less active than the non-heat-treated or 400°C heat-treated samples (Fig. 22).

The O_2 reduction polarization curves for polymeric CoPc/XC-72 showed practically no difference in activity between the non-heat-treated sample and 400°C heat-treated sample. However, the material that was heat-treated at 800°C showed reduced activity, particularly at higher current densities which

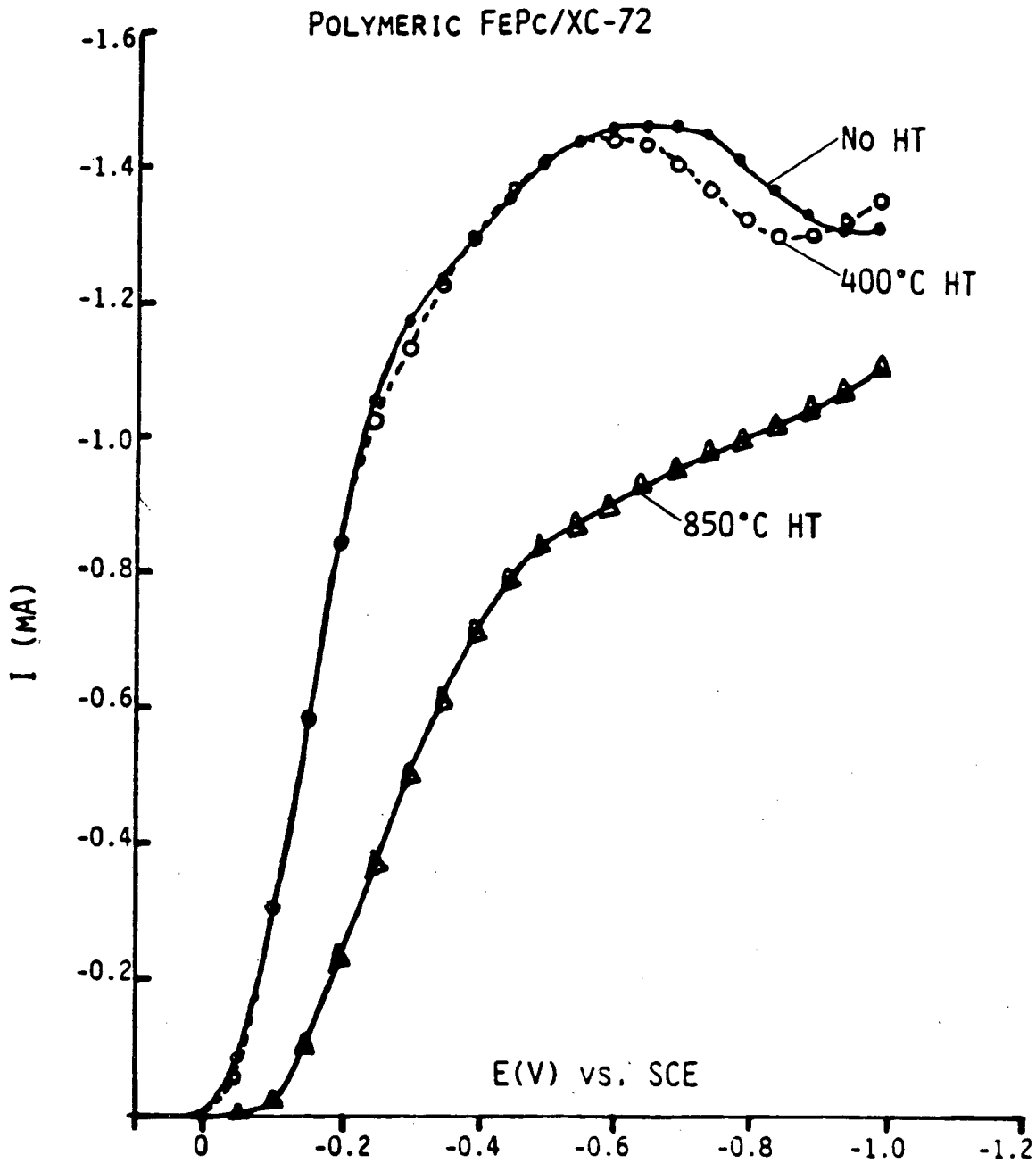

FIG. 22. DISK CURRENTS FOR O_2 REDUCTION (1 ATM) ON A THIN POROUS COATING (TPC) ELECTRODE CONTAINING 5% FEPC(P) ON XC-72 HEAT-TREATED AT DIFFERENT TEMPERATURES IN 0.1 M NAOH. ELECTRODE AREA GEOMETRICAL = 0.2 CM^2, 2500 RPM, ROOM TEMPERATURE, TEFLON = 10%.

may be due to ohmic loss or mass transport limitations. Similar results were obtained for heat-treated polymer FePc which, however, showed larger differences in activity for the heat-treated sample (850°C). This may be due to the decomposition of the polymer at ~850°C and loss of nitrogen which is an essential component along with the metal for the catalytic activity. This is supported by the XPS measurements which show practically no nitrogen 1S peak for the polymeric FeFc/XC-72 heat-treated at 850°C. However, further studies are underway to ascertain the cause of the reduction in activity for heat-treated polymeric phthalocyanines.

2. Heat-treated pyrochlore catalyst

It is shown from the gas-fed electrode measurements that the catalytic activity of the pyrochlore $Pb_2Ru_2O_{6.5}$ decreases both for O_2 reduction and generation with an increase in heat treatment temperature of the catalyst. This diminution in activity is probably due to the decrease in the surface area of the catalyst heat-treated at higher temperatures. The stability of the heat-treated pyrochlore in concentrated alkaline solutions under anodic polarization, however, is expected to increase.

F. Bifunctional Oxygen Electrodes and Improved Catalyst Supports

1. Bifunctional electrodes

The catalysts which were examined during the past year in the bifunctional mode have focused on pyrochlores alone and also in combination with heat-treated macrocycles (Table IV). The pyrochlores in fact have the highest O_2 generation activity of any catalyst examined thus far at CWRU. These pyrochlores were physically mixed with carbon black or heat-treated macrocycles supported carbon. Some of the pyrochlores were also used in a self-supporting mode without carbon, which is generally considered to be unstable, particularly in O_2 generation.

TABLE IV

O_2 Reduction and Generation Polarization Data*
for Pyrochlores Synthesized and Used in the CWRU Research

No.	Compound	carbon or macrocycle on carbon	potentials vs. Hg/HgO, OH^- at the current densities given below in mA cm^{-2} -10	-100	-800	+10
1	$Pb_2Ru_2O_{6.5}$	SB (air ox.)	+30	-95	-195	+525
2	$Pb_2[Ru_{1.67}Pb_{0.33}]O_{6.5}$	SB (air ox.)	+32	-15	-150	+476
		SB (air ox.)/ RAI membrane	+45	-23	-175	+422
		CoTMPP/SB	+38	-32	-125	+465
		CoTMPP/SB/RAI membrane.	+35	-38	-158	+450
		SB (air ox.)/ DDAC/Nafion	+36	-15	-108	+463
3	$Pb_2Ru_2O_{6.5}$	SB (air ox.)	+20	-65	-185	+473
		self supported	+75	+12	-280	+460
4	$Pb_2Ru_{1.5}Ir_{0.5}O_{7-y}$	SB (air ox.)	+35	-31	-172	+483
5	$Pb_2[Ru_{1.8}Pb_{0.2}]O_{6.5}$	SB (air ox.) (no HT)	(unstable)			+446
		280°C HT	-30	-102	-220	+450
6	$Pb_2[Ru_{1.0}Pb_{1.0}]O_{6.5}$	SB (air ox.)	-45	-148	<-350	-
7	$Pb_{1.5}Co_{0.5}Ru_2O_{7-y}$	SB (air ox.)	-10	-60	-190	+472
8	$Y_2Ru_2O_7$	SB (air ox.)	-35	-119	-218	+510
9	$Dy_2Ru_2O_7$	SB (air ox.)	-65	-116	-200	+620
10	$Pb_2Ru_2O_{6.5}$	SB (air ox.)	+5	-77	-220	+448
11	$Bi_{1.5}Co_{0.5}RuIrO_{7-y}$	SB (air ox.)	-78	-130	-230	+555
		CoTMPP/SB	-35	-65	-109	+573
12	$Pb_2Ru_{1.2}Ir_{0.8}O_{7-y}$	SB (air ox.)	+32	-41	-168	+469

* These measurments were made in O_2-saturated 5.5 M KOH at 22°C using porous gas-fed electrodes containing 15.8 mg cm^{-2} pyrochlore, 14.6 mg cm^{-2} air-oxidized Shawinigan black and 6.6 mg cm^{-2} Teflon T30B. The self-supporting electrode contained 54.2 mg cm^{-2} pyrochlore and 4.1 mg cm^{-2} Teflon.

The pyrochlores used in this study can be grouped in six categories (see Table IV): a) Pb substitution in the B sites, b) Ir substitution in the B sites, c) Co substitution in the A sites, d) rare earth substitution in the A sites, e) pyrochlores with ionically conducting polymers, and f) pyrochlores with heat-treated transition metal macrocycles. Below are the specific findings in each area. References to particular numbered compounds and the potentials at some current densities are given in Table IV.

a. Pb substitution in the B sites:

These are the well-known type $Pb_2[Ru_{2-x}Pb_x]O_{6.5}$. Two materials, 1(x=0) and 2(x=0.33), were obtained from Exxon. Others, 3(x=0), 5(x=0.2), 6(x=1.0) and 10(x=0), were prepared at CWRU. No. 10 ($Pb_2Ru_2O_{6.5}$) was prepared in high area form (35 m^2g^{-1}) using the Exxon solution technique. The XRD was qualitatively correct, but the lattice parameter must be checked to determine if it is consistent with this stoichiometry. The X-ray energy-dispersive spectroscopy should also be run to check the stoichiometry. The O_2 generation behavior was excellent, being one of the best tested thus far. Other stoichiometric pyrochlores, 1 and 3, were less active. For O_2 reduction, 2 (55 m^2g^{-1}) obtained from Exxon, performed the best but degraded by dissolution which occurred during anodic polarization measurements. Other O_2 reduction polarization curves for 1, 3, 5 and 10 were rather similar to each other. Sample 3 ($Pb_2Ru_2O_{6.5}$, 6 m^2/g) surprisingly had a slight edge and 6 (x = 1.0) was considerably worse.

b. Ir substitution in the B sites: $Pb_2[Ru_{2-z}Ir_z]O_{7-y}$

Iridium was substituted in the B sites in an attempt to increase stability and activity. The two preparations, with z=0.5 (No. 4) and z=0.8, (No. 12) showed similar activity in both O_2 reduction and generation, but slightly better than 3 (z = 0). The stability could not be ascertained in our short-

term testing.

c. Co substitution in the A sites:

Cobalt is often a constituent in O_2 reduction and generation catalyst. Beck and Kemmler-Sack [30] reported on the synthesis of pyrochlores with Co and other transition metals substituted for Pb and Bi in the A sites. The compounds prepared at CWRU were similar to those reported by Beck and Kemmlersack. These workers, however, did not examine their compounds for O_2 electrocatalysis. Both the O_2 reduction and generation behavior for 7 were very similar to that for 3, while 11 was significantly worse, probably because of its low surface area expected from the 950°C heat treatment.

d. Rare earth substitution in the A sites:

Compounds synthesized with Y and Dy in the A sites (8 and 9, respectively) were inferior to 3 for both O_2 reduction and generation, possibly due to expected poor conductivity.

e. Pyrochlores together with ionic conductive polymers:

Because many of these compounds are susceptible to anodic dissolution it is very desirable to prevent soluble species from leaving the porous electrode. A partially fluorinated anion exchange membrane material (RAI 4035) was pressed onto the electrolyte side of an electrode made from 2 and SB carbon. The O_2 reduction behavior was very similar to that obtained without the membrane (Fig. 23), but the O_2 generation behavior was considerably improved (Fig. 24). The appearance of soluble dissolution products was also impeded somewhat. A similar but smaller effect was observed for an electrode onto which was painted a hydrogel suspension, which was made up using a mixture of poly (dimethyldiallyl) ammonium chloride and Nafion (Figs. 23 and 24). The latter electrode, however, performed very well at high current densities, giving the lowest overpotential yet seen for a metal-oxide-based electrode at -800 mA/cm^2 -108 mV vs. Hg/HgO, OH^-. It performed as well as the best macrocycle + pyro-

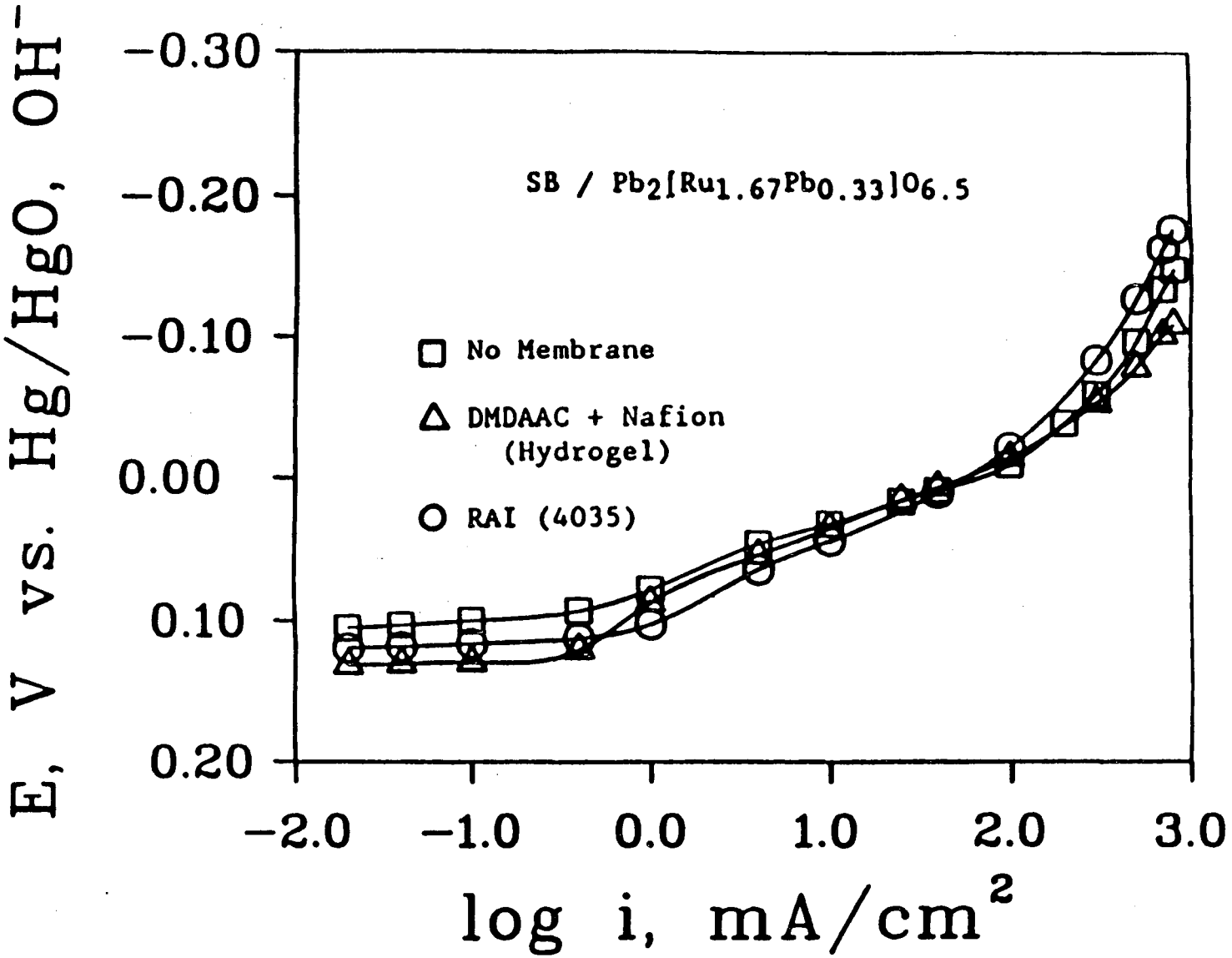

Fig. 23. Polarization curves for O_2 reduction with porous O_2-fed (1 atm) electrodes in 5.5 M KOH at 25°C. The preparation of the hydrogel coating for curve 2 is described in the text. The RAI membrane was pressed onto the solution side of the electrode

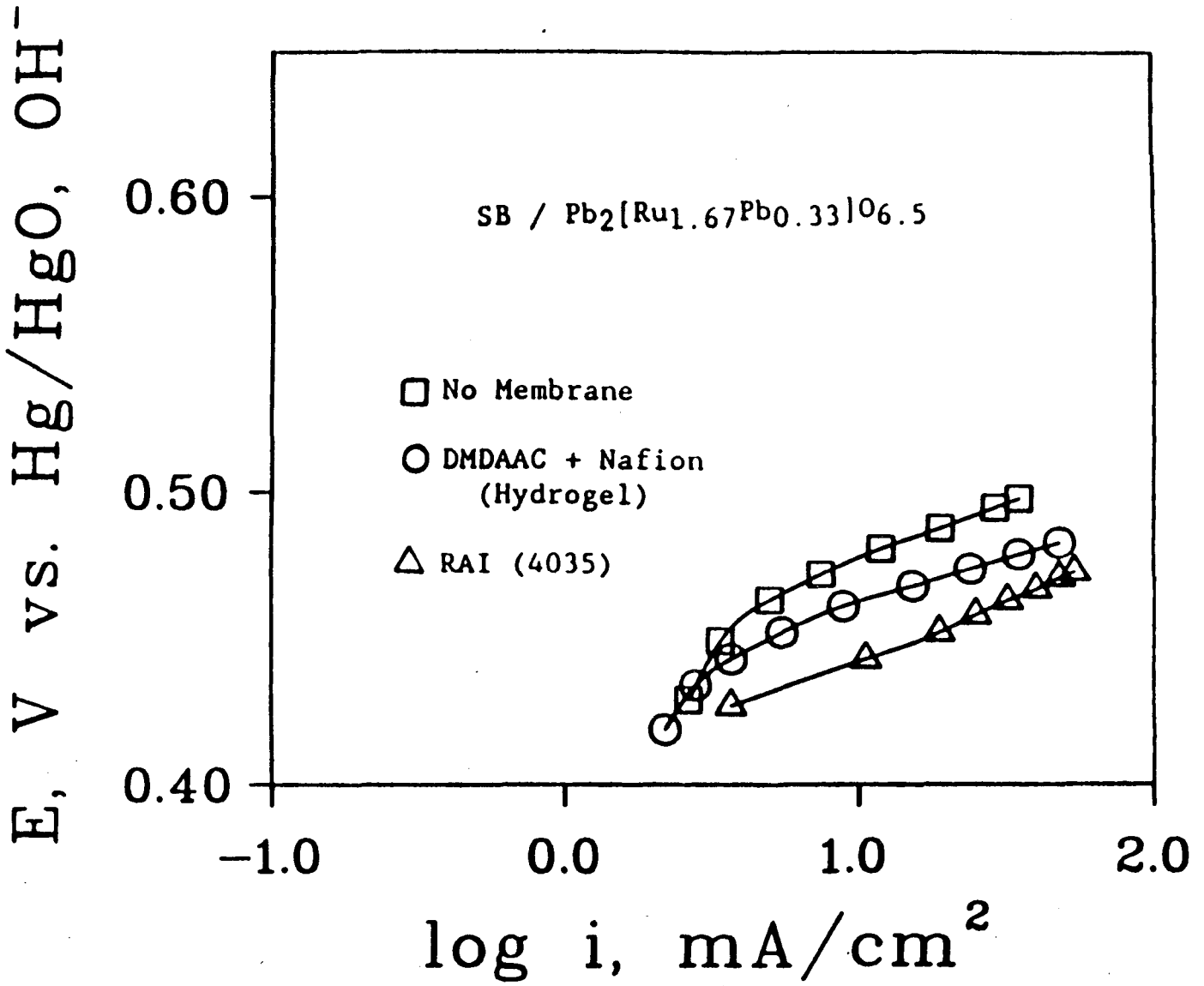

FIG. 24. POLARIZATION CURVES FOR O_2 GENERATION WITH POROUS O_2-FED (1 ATM) ELECTRODES IN 5.5 M KOH AT 25°C. THE ELECTRODE CONTAINED 15.8 MG/CM^2 PYROCHLORE, 15.0 MG/CM^2 AIR-OXIDIZED SHAWINIGAN ACETYLENE BLACK AND WAS HEAT-REATED AT 280°C FOR 2 H IN FLOWING MEDIUM.

chlore, 11.

f. Pyrochlores with transition metal macrocycles:

The use of such macrocycles (heat-treated on carbon) instead of the usual air-oxidized SB carbon usually leads to O_2 reduction behavior which is typical of the macrocycle, i.e. Tafel linearity with slopes of -35 to -40 mV/decade, but with a slight enhancement in activity due possibly to improved peroxide decomposition. The O_2 generation behavior of the pyrochlore is not affected by the presence of the macrocycle. These expectations were largely borne out, except that, with 2 mixed with CoTMPP/SB. There was an unexpectedly large increase in the O_2 reduction overpotential at very low cd, (~+200 mV vs. Hg/HgO, OH^- at cd below 0.1 mA/cm^2).

There has only been one test of a self-supported pyrochlore, i.e., one without carbon. That was with 2, which showed that the low-cd behavior for the self-supported catalyst is better than that with carbon but is worse at high cd (Figs. 25 and 26). The better low-cd behavior is probably due to the lack of a carbon oxidation current and consequently larger amount of wetted catalysts, and the poorer high cd behavior is probably because of the lack of an optimized electrode structure, leading to ohmic and/or mass transport problems. In the near future, much more work will be carried out with self-supporting pyrochlores without carbon since carbon oxidation is a major problem in the O_2 generation mode.

2. Improved catalyst supports

Most of the high-area carbons which are used as the support material for the catalysts are generally considered to be unstable, particularly in the O_2 generation mode. Efforts have been made to find improved carbon supports. Experiments (O_2 reduction and generation) were conducted on heat-treated (450°C) metal-free teramethoxyphenyl porphyrin (H_2TMPP) supported on Lawrence

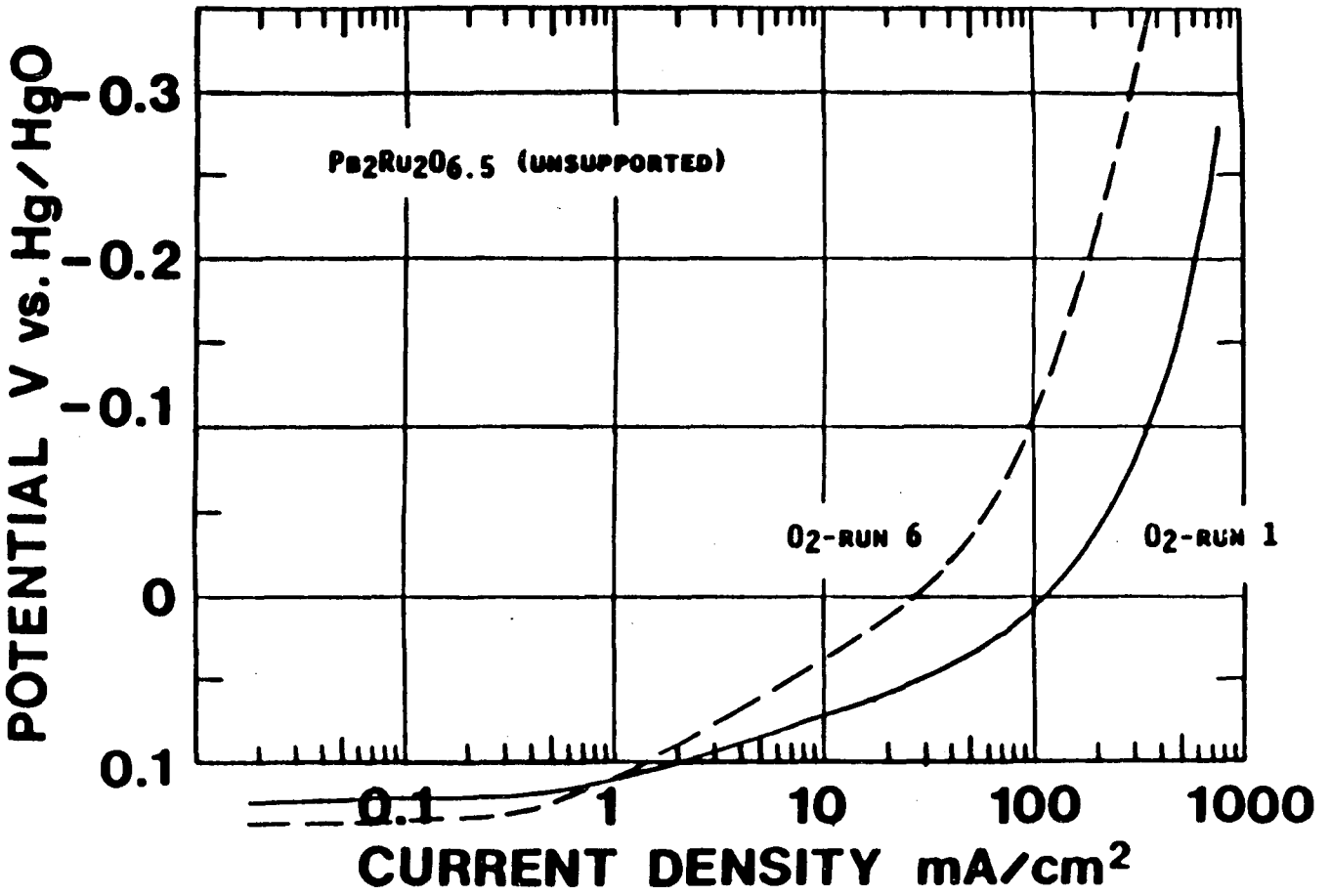

FIG. 25. POLARIZATION CURVES FOR O_2 REDUCTION WITH A GAS-FED (1 ATM) ELECTRODE IN 5.5 M KOH AT 22° C. THE ELECTRODE CONTAINED 54.2 MG/CM^2 PYROCHLORE AND 4.1 MG/CM^2 TEFLON T30B AND WAS HEAT-TREATED AT 270°C FOR 2 H IN FLOWING HELIUM.

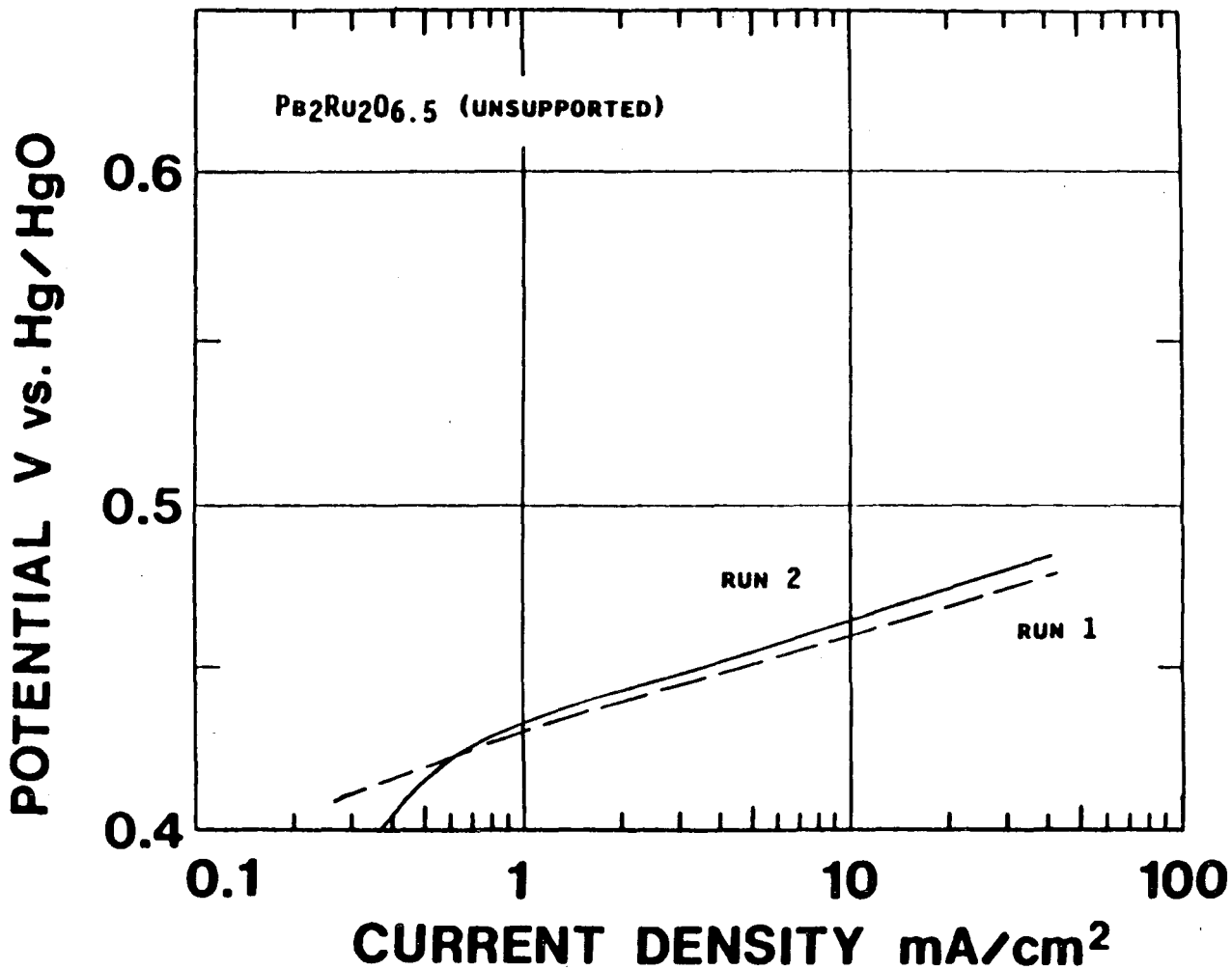

FIG. 26. POLARIZATION CURVES FOR O_2 GENERATION WITH A GAS-FED (1 ATM) ELECTRODE IN 5.5 M KOH AT 22° C. THE ELECTRODE CONTAINED 54.2 MG/CM² PYROCHLORE AND 4.1 MG/CM² TEFLON T30B AND WAS HEAT-TREATED AT 270° C FOR 2 H IN FLOWING HELIUM.

Berkeley Laboratory (LBL) carbon supplied by Dr. Phil Ross and mixed with the perovskite $LaFe_{0.15}Ni_{0.85}O_3$. The activity was found to be poor particularly for O_2 generation. The LBL carbon was expected to be more oxidation resistant and hence more suitable for O_2 generation than the other high-area carbons.

Preliminary experiments were also conducted with mildly fluorinated SB carbon (Electrosynthesis Company, Inc., NY) as the support material. No improvements in O_2 reduction behavior were observed for the mildly fluorinated SB carbon alone or CoTMPP-catalyzed mildly fluorinated SB carbon, as compared to the oxidized SB carbon alone or the CoTMPP-catalyzed SB carbon, respectively. However, work is in progress to ascertain the effect of mild fluorination of high area carbons on the activity and stability of such carbons for O_2 reduction and generation with and without catalysts present on such supports. Efforts are also being made to mildly fluorinate the heat-treated macrocycles on high area carbons and their characterization.

V. FUTURE WORK

1. Further examination of the structure and orientation of the adsorbed macrocycle films on HOPG and OPG including EXAFS studies for the non-heat-treated and heat-treated macrocycles on carbon.
2. Controlled poisoning of macrocycles by CO.
3. Adsorbed layers of mixtures of macrocycles on graphite and carbon surfaces and their role in promoting the 4-electron reduction of O_2.
4. Solid ionomer polymeric coatings for O_2 reduction.
5. O_2 reduction and generation with pyrochlores and other oxide catalysts.
6. Alternative and modified catalyst supports.

VI. REFERENCES

1. S. L. Gupta, I. T. Bae, R. R. Chen, B. Simic-Glavaski and E. Yeager, Vol. 88-1, p. 524, The National Meeting of the Electrochemical Society, Atlanta May 1988, Extended Abstract No. 355.

2. B. Simic-Glavaski, S. Zecevic and E. Yeager, J. Am. Chem. Soc., 107, 5725 (1985).

3. P. H. Lippel, R. J. Wilson, M. D. Miller, Ch. Woll and S. Chiang, Phys. Rev. Letters, 62, 171 (1989).

4. B. A. Achar, G. M. Fohler and J. A. Parker, J. Polymer Sci., 20, 1785 (1982).

5. J. D. E. McIntyre, in "Advances in Electrochemistry and Electrochemical Engineering", P. Delahey and C. W. Tobias Eds., John Wiley & Sons, NY, 1973, Vol. 9.

6. A. Tadjeddine, Electrochim. Acta, 34, 29 (1989).

7. P. W. Faguy, N. Markovic, R. Adzic and E. Yeager, to be published.

8. I. T. Bae and E. Yeager, unpublished results.

9. B. Z. Nikolic, R. R. Adzic and E. B. Yeager, J. Electroanal. Chem., 103, 281 (1979).

10. E. Yeager, "Electrocatalysts for Oxygen Electrodes", Annual Report, LBL No. 26054, prepared by the Case Western Reserve University for Lawrence Berkeley Laboratory, CA, August, 1988, p. 26.

11. A. J. Bard and L. R. Faulkner, "Electrochemical Methods", Fundamental and Applications, John wiley & Sons, NY, 1980.

12. I. T. Bae, Ph.D. Dissertation, Case Western Reserve University, July, 1989.

13. R. Holze, Electrochim. Acta, 33, 1619 (1988).

14. R. D. Jones, D. A. Summerville and F. Basolo, Chem. Rev., 79, 139 (1979) and references therein.

15. E. Yeager, S. L. Gupta, B. Simic-Glavaski and I. T. Bae, The National Meeting of the Electrochemical Society, Los Angeles, May 1989, Extended Abstract No. 477.

16. I. T. Bae, X. Xing, E. Yeager and D. Scherson, Anal. Chem., 61, 1164 (1989).

17. I. T. Bae, X. Xing, C. C. Liu and E. Yeager, J. Electroanal. Chem., submitted.

18. J. Zagal, P. Bindra and E. Yeager, J. Electrochem. Soc., 127, 1506 (1980).

19. S. Zecevic, B. Simic-Glavaski, E. Yeager, A. B. P. Lever and P. C. Minor, J. Electroanal. Chem., 196, 338 (1985).

20. W. A. Nevin, W. Liu, M. Melnik and A. B. P. Lever, J. Electroanal. Chem., 213, 217 (1986).

21. A. B. P. Lever, and J. P. Wilshire, Inorg. Chem., 17, 1145 (1978).

22. A. Tanaka, Ph.D. Dissertation, Case Western Reserve University, 1987.

23. D. Scherson, S. L. Gupta, C. Fierro, E. B. Yeager, M. E. Kordesch, J. Eldrige, R. W. Hoffman and J. Blue, Electrochim. Acta, 28, 1205 (1983).

24. S. Gupta, D. Tryk, M. Daroux, W. Aldred and E. Yeager, in 'Proceedings of the Symposium on Load Levelling and Energy Conservation in Industrial Processes', edited by D. Chin, The Electrochemical Society, Pennington, NJ (1986) p. 207.

25. H. S. Horowitz, J. M. Longo and N. H. Horowitz, J. Electrochem. Soc., 130, 1851 (1983).

26. P. E. Edgell, J. B. Goodenough, A. Hammet and C. C. Naish, J. Chem. Soc., Farady Trans., I, 79, 893 (1983).

27. C. Iwakura, T. Edemoto and H. Tamura, Bull. Chem. Soc., Japan, 59, 145 (1986).

28. H. S. Horowitz, J. M. Longo and J. T. Lewandowski, Mater. Res. Bull., 16, 4889 (1981).

29. J. A. R. Van Veen, J. M. Van Der Eijk, P. De Ruiter and S. Huizinga, Electrochim. Acta, 33, 51 (1988).

30. E. Beck and S. Kemmler-Sack, J. Less Common Metals, 113, 65 (1985).

LAWRENCE BERKELEY LABORATORY
TECHNICAL INFORMATION DEPARTMENT
1 CYCLOTRON ROAD
BERKELEY, CALIFORNIA 94720